1,4-Diethynylbenzene-Bridged [Cp*(dppe)Fe](n+) Units: Effect of 2,5-Ethynyl Groups on the Chemical and Electronic Properties

Rim Makhoul, Thomas Groizard, Paul Hamon, Thierry Roisnel, Vincent Dorcet, Samia Kahlal, Jean-François Halet, Jean-René Hamon, Claude Lapinte

10.1002/ejic.202000345

WILEY-VCH

1,4-Diethynylbenzene-Bridged $[Cp^*(dppe)Fe]^{n+}$ Units: Effect of 2,5-Ethynyl Groups on the Chemical and Electronic Properties

Rim Makhoul,[a] Thomas Groizard,[a] Paul Hamon,[a] Thierry Roisnel,[a] Vincent Dorcet,[a] Samia Kahlal,[a] Jean-François Halet,*[a] Jean-René Hamon,*[a] and Claude Lapinte*[a]

Dedicated to our friend Prof. Maria José Calhorda on the occasion of her 70th birthday.

Abstract: The bis(ironvinylidene) complex [1,4-{Cp*(dppe)Fe=C=CH}$_2$-2,5-(C≡CH)$_2$-C$_6$H$_2$](PF$_6$)$_2$ (**[2-2H](PF$_6$)$_2$**) was prepared from 1,2,4,5-tetraethynylbenzene and two equiv of Cp*(dppe)FeCl in 87% yield. The reaction is very selective and **[2-2H](PF$_6$)$_2$** is the unique organoiron species to be formed. Deprotonation of **[2-2H](PF$_6$)$_2$** provided the target complex **2** (66 % yield) and subsequent oxidation gave the monocationic and dicationic complexes **2(PF$_6$)** and **2(PF$_6$)$_2$**. The new complexes were characterized by ESI-mass spectrometry, IR, multinuclear NMR, ESR and Mössbauer spectroscopies, and XRD analyses on single crystals for **[2-2H](PF$_6$)$_2$** and **2(PF$_6$)$_2$**. The magnetic properties of **2(PF$_6$)$_2$** were investigated by VT ^{1}H NMR. The data were analyzed with the support of quantum chemistry calculations. The terminal ethynyl groups on the aromatic ring of the bridge modify the population of the bridge-oxidized state, weaken the electronic communication (H_{ab} ≈ 601 cm^{-1}) and strengthen magnetic coupling interactions (J = -530 cm^{-1}) compared to the unsubstituted species (H_{ab} = 1700 cm^{-1} and J = -530 cm^{-1}, respectively).

Introduction

Development of molecules as components for molecular electronics devices has attracted sustained interest over decades as means of achieving miniaturization of integrated circuits.[1, 2] Among them, nanometer-sized π-conjugated molecular wires are suitable candidates owing to their delocalized electrons and small HOMO-LUMO gaps.[3-6] In particular, a large variety of molecules composed of two redox-active organometallic termini connected by a carbon-rich extended π-system has been developed.[7-23] The wire-like performance of these compounds has been largely investigated by means of various physical methods[8, 24-30] including scarce measurements at the molecular level.[31-38]

The exploration of novel conjugated architectures is yet a productive area of current research.[39-46] In this context, the design of transition-metal compounds with cross-conjugated alkynyl ligands opened new perspectives. In the last decade, different two-dimensional, X-shaped conjugated materials have been synthesized for a variety of applications.[47] Cross-conjugation was defined as the conjugation between two unsaturated π-segments which are not conjugated to each other, but rather conjugated to bridging unsaturated segment.[39] Among the various possible structures of bridging ligands,[48] these organometallics are mostly constructed from two intertwined π-conjugated linear arms through a central *geminal*-diethynylethene,[39-42, 49] a tetraethynylethene,[50, 51] or an aromatic core.[52-55]

Understanding electron–hole delocalization and transfer processes over two-dimensional (2D) skeletons with four metal sites is important for the development of molecular devices, such as quantum cellular automata,[56-58] phase-coherent logic gates, and some designs of single-molecule transistors.[59] As a prerequisite for the construction of more complex derivatives containing more than two redox active centers, we have focused our interest on the perturbation produced by the introduction of two ethynyl groups in the previously studied complexes [1,4-{Cp*(dppe)FeC≡C}$_2$-C$_6$H$_4$](PF$_6$)$_n$ (***p*-1(PF$_6$)$_n$**, n = 0-2, Scheme 1).[60] It is interesting to recall that we recently reported the synthesis of the sterically hindered complexes [1,2-{Cp*(dppe)FeC≡C}$_2$-C$_6$H$_4$](PF$_6$)$_n$ (***o*-1(PF$_6$)$_n$**, n = 0-2, Scheme 1).[61] Despite strong steric constraints between the *ortho* organoiron fragments, which are at the origin of a strong chemical inertness, this work demonstrates that introduction of substituents on the 2,5-positions of the central aromatic ring in ***p*-1** constitutes a viable synthetic target.

For this purpose, the new complexes [1,4-{Cp*(dppe)FeC≡C}$_2$-2,5-(C≡CH)$_2$-C$_6$H$_2$](PF$_6$)$_n$ (**2**, n = 0-2) were prepared and characterized by various means including X-ray diffraction on single crystals of the bis-vinylidene precursor **[2-2H](PF$_6$)$_2$** and the bis-iron(III) complex **2(PF$_6$)$_2$**. Investigation of the electronic and magnetic properties of these new complexes with a wide range of spectroscopic techniques and quantum chemistry calculations carried out at the density-functional theory (DFT) level shows the critical effect of the *ortho* C≡CH substituents on the acid-base properties of the iron-alkynyl moieties and the electronic and magnetic interactions between the spin carriers in the mono- and dicationic derivatives, respectively.

[a] Univ Rennes,
CNRS, ISCR-UMR 6226,
35000 Rennes, France
E-mail: jean-françois.halet@univ-rennes1.fr
jean-rene.hamon@univ-rennes1.fr
claude.lapinte@univ-rennes1.fr
https://iscr.univ-rennes1.fr/

Supporting information and ORCID(s) from the authors for this article are given via a link at the end of the document.

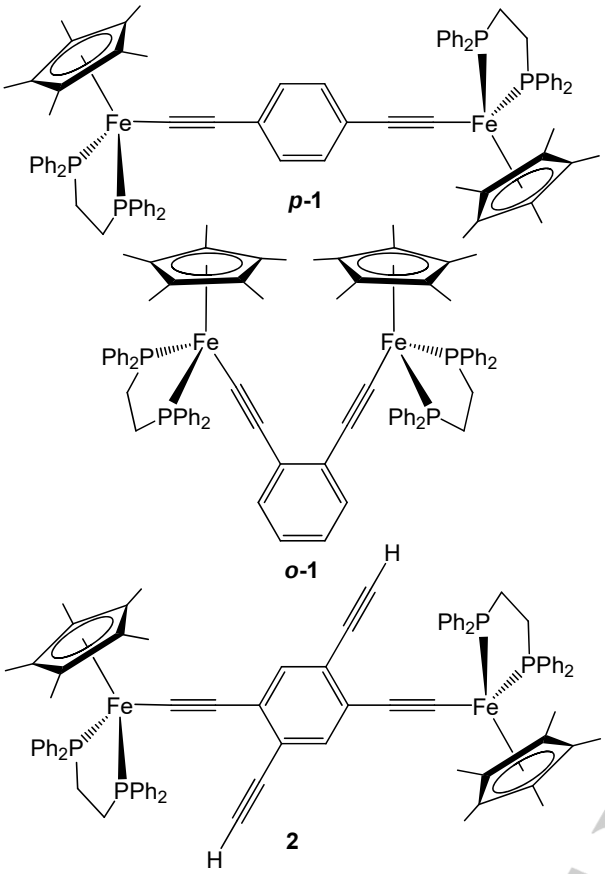

Scheme 1.

that 1,2-bis-ethynylbenzene reacts with the chloro-iron complex **3** to give the *ortho*-branched bis(iron-vinylidene) complex [1,2-{(Cp*(dppe)Fe=C=CH-}$_2${C_6H_4}](PF$_6$)$_2$.[61] This assumption was also confirmed by an additional experiment. The reaction depicted in Scheme 2 was reproduced using a fivefold excess of Cp*(dppe)FeCl and carried out during 48 h at 50 °C. Again, the complex **[2-2H](PF$_6$)$_2$** was the unique product formed during the reaction. The presence of any organometallic compounds containing more than two iron centers was not detected by mass spectrometry. The tetrairon derivative can, however, be generated under other specific experimental conditions.[57]

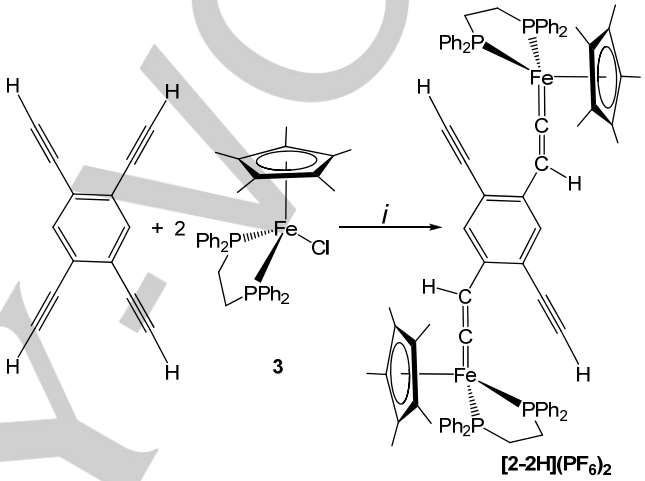

Scheme 2. Synthesis of complex **[2-2H](PF$_6$)$_2$**. Key reagents: i) NH_4PF_6, MeOH, THF, 16 h, 20 °C.

Results and Discussion

1. Synthesis of the Bis(ironvinylidene) Complex [1,4-{Cp*(dppe)Fe=C=CH-}$_2$-2,5-(C≡CH)$_2$-C$_6$H$_2$](PF$_6$)$_2$ ([2-2H](PF$_6$)$_2$)

Treatment of freshly prepared 1,2,4,5-tetraethynylbenzene with 2 equiv of Cp*(dppe)FeCl (**3**) in a 2:1 MeOH/THF mixture and in the presence of NH_4PF_6 provided the (1,4-bis-ironvinylidene)(2,5-bis-ethynyl)benzene complex **[2-2H](PF$_6$)$_2$** isolated as brown yellow crystals in 87 % yield after 16 h of reaction (Scheme 2). The reaction is very selective and complex **[2-2H](PF$_6$)$_2$** is the unique organoiron species formed. The iron vinylidene and terminal alkyne groups were identified by their FTIR signatures ($\nu_{FeC=C}$ = 1621 cm^{-1}, $\nu_{C\equiv C}$ = 2100 cm^{-1}, KBr). The new organoiron derivative was isolated in a pure form and characterized by ^{1}H, ^{13}C, and ^{31}P NMR, and its molecular structure was established by X-ray diffraction on a single crystal.

It is of interest to emphasize the regiospecificity of the reaction of complexation of the 1,2,4,5-tetraethynylbenzene which gave **[2-2H](PF$_6$)$_2$** as a unique product. It can be assumed that this reaction is both under charge and steric controls. The steric hindrance should favor the 1,4 geometry because of the bulkiness of the organoiron fragments, and the repulsion between the positive charges should limit the complexation to two iron moieties. In accord with this hypothesis, it was found

2. Synthesis of the Bis(iron(II) Acetylide) Complex [1,4-{Cp*(dppe)Fe-C≡C-}$_2$-2,5-(C≡CH)$_2$-C$_6$H$_2$] (2)

Generally, the deprotonation of vinylidene-iron and bis(vinylidene-iron) complexes is quantitatively achieved using a stoichiometric amount of KOBu^t.[11, 60, 62] It was found that the reaction reached completion in 1 h or less, except in the particular case of the sterically hindered complex [1,2-{Cp*(dppe)Fe=C=CH}$_2$-C$_6$H$_4$](PF$_6$)$_2$ for which the reaction needs 72 h to complete. It was considered that the chemical inertness reflects the steric constraints involved in the transformation of the bis(vinylidene) into the bis(alkynyl) complex.[61]

Following the usual procedure, complex **[2-2H](PF$_6$)$_2$** was reacted with a small excess (2.5 equiv) of KOBu^t in THF at 20 °C. After 16 h of reaction, the solvent was removed and the crude residue was analyzed by IR spectroscopy. The disappearance of the band at 1621 cm^{-1} confirmed that all the starting material was consumed and that the presence of a new band at 2046 cm^{-1} is consistent with the formation of the expected product **2**. However, the spectrum also displays two strong and unexpected bands at 2028 and 1568 cm^{-1} indicating the presence of a second complex identified as **[2-H](PF$_6$)** (Scheme 3). The relative intensities of the two groups of bands are independent of the time of reaction (16 h - 48 h) and of the number of equivalents of KOBu^t (ranging from 2 to 5 equiv) employed.

Extraction with toluene, allowed the separation of **2** and [**2-H](PF$_6$)**. The IR spectrum of the insoluble fraction shows a band at 2046 cm^{-1}, while the IR spectrum of a powdered sample of the soluble compound displays characteristic bands at 2028 and 1568 cm^{-1}. Despite its reasonable solubility in toluene, this compound is a salt which presents the characteristic signature of the PF_6^- anion at 840 cm^{-1}. On the basis of the spectroscopic data, complex **[2-H](PF$_6$)** results from the monodeprotonation of its bis(vinylidene) parent. In solution in C_6D_6, the ^{31}P NMR spectrum shows two singlets at δ 99.8 and 101.3 ppm with similar integral and a heptet at δ -144.0 ppm corresponding to the PF_6^- anion. Surprisingly, an intermediate resonance at δ 100.5 ppm of lower intensity is also observed. The presence of the latter resonance assigned to the neutral complex **2** (see below) in the spectrum of **[2-H](PF$_6$)** indicates that **2** and **[2-H](PF$_6$)** are in equilibrium. The resonance corresponding to the dppe ligand on the vinylidene side is very much up-field shifted with respect to the value observed for the related compound **[2-2H](PF$_6$)$_2$** (δ 86.20), suggesting that the C_β-H bond is weakened and strongly polarized. This is also supported by the presence in the solution of the neutral complex **2**, which was not observed by IR in the solid state.

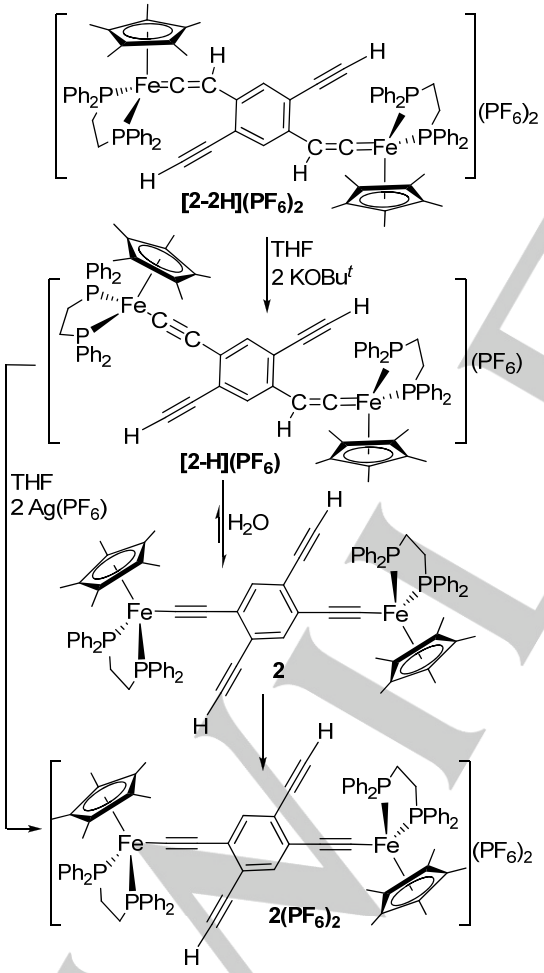

Scheme 3. Syntheses of **[2-H](PF$_6$)**, **2**, and **2(PF$_6$)$_2$**.

The target complex **2** can be obtained from the treatment with water of a CH_2Cl_2 suspension of the crude residue **[2-H](PF$_6$)**. As the reaction proceeded, complex **2** precipitated from the solution. After removal of the solvent, washing with ethanol and pentane, and drying under reduced pressure, the new complex **2** was isolated in 66 % yield as an orange powder, which is thermally stable under argon atmosphere. Note that a one-pot procedure allowed the preparation of **2** directly from **[2-2H](PF$_6$)$_2$** with the same yield (see Experimental Section). The structure was identified by its $\nu_{(C\equiv CH)}$ and $\nu_{(FeC\equiv C)}$ bands at 2100 and 2045 cm^{-1}, respectively in the IR spectrum (KBr). The extreme insolubility of **2** rendered very difficult all efforts of purification and characterization in solution. However, we established that **2** is characterized by a unique singlet in the ^{31}P NMR spectrum at δ 100.5 ppm. The signature of the Cp* ligand was also unequivocally found in the ^{1}H NMR spectrum at δ 1.55 ppm (C_6D_6).

The deprotonation reaction of the bis(vinylidene) complex **[2-2H](PF$_6$)$_2$** compares neither with any other related reactions performed with mono-, bi- and tri-nuclear iron vinylidene species already reported for the Cp*(dppe)Fe series nor with similar reactions previously reported for d^6 complexes.[11, 60, 62, 63] It is difficult to explain this particular and unprecedented behavior assuming a weak and specific interaction of the vinylic protons with the C≡CH acetylide groups, since the $\nu_{C\equiv CH}$ IR stretches are exactly at the same energy in **[2-2H](PF$_6$)$_2$** and **2**. Possibly, the presence of the acetylide groups strengthens the anion-cation-solvent interactions and addition of water breaks the ion-pairing association.

3. Synthesis of the Bis(iron(III) Acetylide) Complex [1,4-{Cp*(dppe)Fe-C≡C-}$_2$-2,5-(C≡CH)$_2$-C$_6$H$_2$](PF$_6$)$_2$ (2(PF$_6$)$_2$)

The dicationic complex **2(PF$_6$)$_2$** can be obtained almost quantitatively by treatment of **2** with two equiv of [Cp$_2$Fe](PF$_6$). However, it is much more advantageous to start from the bis(vinylidene) **[2-2H](PF$_6$)$_2$**. This complex was first reacted with 2 equiv of KOBu^t in THF at 20 °C and after 16 h, 2 equiv of silver hexafluorophosphate were added to the THF suspension (Scheme 3). After stirring the mixture for 4 additional hours, work up and crystallization, complex **2(PF$_6$)$_2$** was obtained in 90 % yield as black-green crystals analytically pure and suitable for X-ray analysis. The high yield obtained for **2(PF$_6$)$_2$** is consistent with an equilibrium between **[2-H](PF$_6$)** and **2** accompanied with HPF_6. As the oxidation of **2** proceeds, the equilibrium is displaced to the formation of **2(PF$_6$)$_2$** until the reaction reaches completion. The doubly oxidized complex was characterized by high-resolution ESI-mass spectrometry, cyclic voltammetry, and IR, Mössbauer, EPR, UV-vis, and NIR spectroscopies. In addition, the magnetic properties of compound **2(PF$_6$)$_2$** were investigated by ^{1}H and ^{31}P NMR spectrometry in solution (see Section 13).

4. Synthesis of the Mixed-Valence Iron(II) Iron(III) Bis(acetylide) Complex [1,4-{Cp*(dppe)Fe-C≡C-}$_2$-2,5-(C≡CH)$_2$-C$_6$H$_2$](PF$_6$) (2(PF$_6$))

The monocationic complex **2(PF$_6$)** can be prepared either by oxidation of the neutral complex **2** with 1 equiv of [Cp$_2$Fe](PF$_6$) in THF (procedure A) or by reaction of 1 equiv of **2** with 1 equiv of the doubly oxidized complex **2(PF$_6$)$_2$** in THF (procedure B). The high insolubility of the neutral complex **2** makes the isolation of the monocationic salt critical. In the case of procedure A, the target compound was isolated by rapid addition of a large amount of pentane under fast stirring to remove the amount of ferrocene formed during the reaction. Depending on the precipitation conditions, it was sometimes observed by IR spectroscopy that traces of **2** and **2(PF$_6$)$_2$** contaminate the samples. Procedure B allowed the isolation of **2(PF$_6$)** by removal of the solvent under reduced pressure. After drying, the monocationic complex **2(PF$_6$)** was quantitatively obtained as a violet powder in a spectroscopically pure form. All efforts of crystallization of the monocationic compound using mixtures of solvents were unsuccessful and invariably gave the same result. Indeed, the extreme insolubility of the neutral derivative **2** acts as the driving force for the precipitation of the neutral form on the bottom of the glassware, while the solutions contain a mixture of the salts **2(PF$_6$)** and **2(PF$_6$)$_2$**. Monocationic complex **2(PF$_6$)** was characterized by high-resolution ESI-mass spectrometry, cyclic voltammetry, and IR, Mössbauer, EPR, UV-vis, and NIR spectroscopies.

5. Cyclic Voltammetry of 2(PF$_6$)$_n$

The insolubility of **2** did not permit electrochemical measurements. The initial scan in the cyclic voltammetry of the new complex **2(PF$_6$)** and **2(PF$_6$)$_2$** were run from -1.0 to 1.0 V [vs standard calomel electrode (SCE)]. As expected, the two complexes displayed the same voltammogram (Figure 1) characterized by two reversible and fully resolved waves with the i_p^a/i_p^c current ratio of unity for the two sequential electron transfers. The electrochemical potentials are collected in Table 1 with those reported for the related compound ***p*-1**. The anodic and cathodic peak separation approaches 0.060 V with a 0.100 V s^{-1} scan rate as expected for fast electron transfer processes.[64]

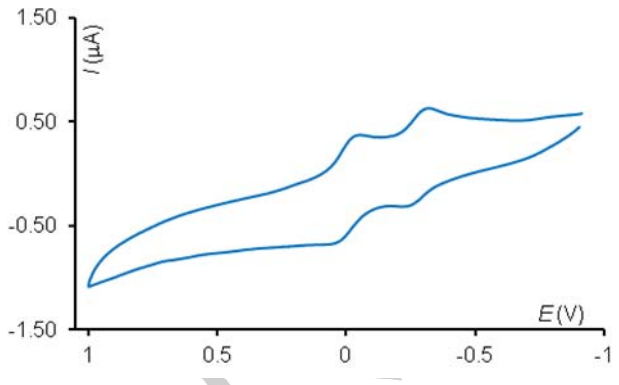

Figure 1. Cyclic voltammogram of **2(PF$_6$)$_2$** (conditions are given in Table 1).

In comparison with complex ***p*-1**, the first oxidation potential is slightly shifted toward negative values by 0.01 V, while the second oxidation potential is shifted toward positive values by the same quantity. As a consequence, the wave separation between the two one-electron processes is 0.02 V larger for **2** than for ***p*-1**. This result reveals that the two alkynyl groups at the central phenyl ring modify in a detectable way the electronic interactions taking place between the two redox active [Cp*(dppe)Fe-C≡C-] fragments. As this effect is in the limit of the experimental accuracy, its origin was not further investigated.

Table 1. Comparison of the Electrochemical Potentials for ***p*-1** and **2**.[a]

compd	E^0_1	E^0_2	$E^0_1 - E^0_2$	K_c	ref
***p*-1**	-0.27	-0.01	0.26	2.5 x 10^4	[60]
2	-0.28	0.00	0.28	5.4 x 10^4	[b]

[a] Potentials in CH_2Cl_2 (0.1 M Bu$^n_4$N](PF$_6$), 25 °C, platinum electrode, sweep rate 0.100 V s^{-1}) are given in V vs SCE; the ferrocene-ferrocenium couple (0.46 V vs SCE)[65] was used as an internal reference for the potential measurements. [b] This work.

6. Molecular Structures of [2-2H](PF$_6$)$_2$•2CH$_2$Cl$_2$ and 2(PF$_6$)$_2$•2CH$_2$Cl$_2$

Slow diffusion of pentane into concentrated solutions of the bis(iron) complexes **[2-2H](PF$_6$)$_2$** and **2(PF$_6$)$_2$** in dichloromethane provided suitable crystals for X-ray analyses. Diffraction parameters for these compounds are collected in Table S1 (Supporting Information). ORTEP views are given in Figure 2, while pertinent distances and angles for these two dicationic complexes are reported in Table 2. In both cases, the asymmetric unit contains half a molecule of the complex, one PF_6^- counteranion and one dichloromethane molecule. In the two structures, the terminal iron fragments have the expected pseudo-octahedral geometry with bond lengths and angles in the previously established ranges.[7, 8, 61]

Complex **[2-2H](PF$_6$)$_2$•2CH$_2$Cl$_2$** crystallizes in the triclinic space group $P\bar{1}$ and has an inversion center. The short Fe=C bond distance (1.748(4) Å) is consistent with a formal double bond character. Slightly longer Fe=C bond lengths (1.76 - 1.78 Å) have been found for mononuclear vinylidene complexes in the same series.[66] In line with this relatively short Fe=C bond, the C37-C38 bond (1.307(6) Å) is found longer than those in the related mononuclear relatives (1.22 - 1.30 Å).[66] As often noted in the X-ray crystal structures of metallacumulenylidene complexes, the Fe1-C37-C38 angle deviates from linearity.[63, 67] The torsion angles Cp*centroid-Fe1-C38-H38 and Cp*centroid-Fe1-C38-C39 are 112.9 and 59.9°, respectively showing that the plane of the vinylidene ligands are not perpendicular to the plane of the Cp* ring. It has been reported on many cases that the electronic preference is often overridden by steric or packing effects.[63]

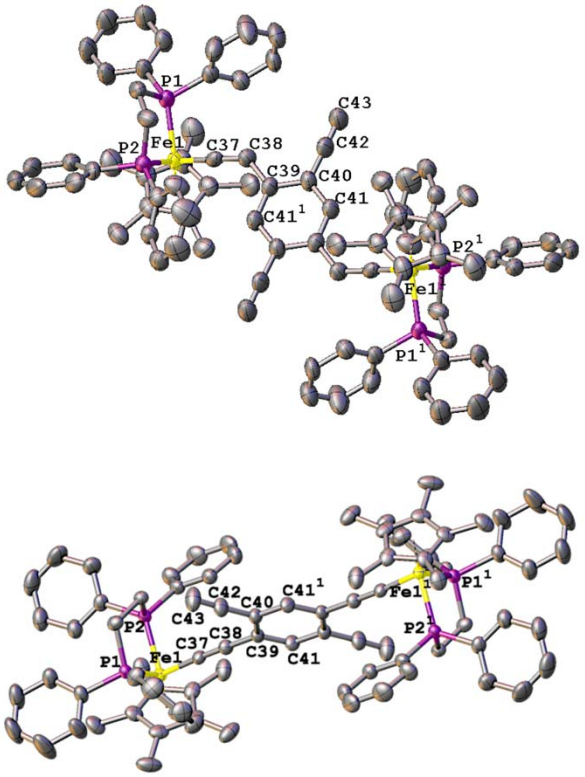

Figure 2. Molecular structures of **[2-2H](PF$_6$)$_2$•2CH$_2$Cl$_2$** (top) and **2(PF$_6$)$_2$•2CH$_2$Cl$_2$** (bottom) with a partial labeling scheme. Hydrogen atoms, counteranions and crystallization solvent molecules have been removed for clarity. Thermal ellipsoids are drawn at 70 % probability. Half unit of both complex were generated by symmetry operations -x, -y, -z and selected equivalent atoms are marked with the symmetry label: [1].

Table 2. Pertinent experimental distances (Å) and angles (°) for **[2-2H](PF$_6$)$_2$•2CH$_2$Cl$_2$** and **2(PF$_6$)$_2$•2CH$_2$Cl$_2$**

compd	**[2-2H](PF$_6$)$_2$•2CH$_2$Cl$_2$**	**2(PF$_6$)$_2$•2CH$_2$Cl$_2$**
Fe1-Cp*[a]	1.785	1.765
Fe1-C37	1.748(4)	1.853(2)
Fe1-P1	2.2485(14)	2.2616(7)
Fe1-P2	2.2223(13)	2.2408(6)
C37-C38	1.307(6)	1.221(3)
C38-C39	1.468(6)	1.414(3)
C39-C40	1.422(6)	1.423(3)
C39-C41	1.392(6)	1.406(3)
C40-C42	1.421(7)	1.435(3)
C42-C43	1.190(7)	1.187(4)
C41-C40[1]	1.402(6)	1.394(3)
Fe1-Fe2	10.886	11.784
P1-Fe1-P2	85.21(5)	84.42(2)
P1-Fe1-C37	91.39 (15)	88.06 (7)
P2-Fe1-C37	85.81(14)	85.68(7)
Fe1-C37-C38	170.3(4)	176.5(2)
C37-C38-C39	131.6(4)	178.2(2)
C38-C39-C40	118.8(4)	121.2(2)
C38-C39-C41	123.3(4)	119.7(2)
C40-C39-C41	117.9(4)	119.13(19)
C39-C41-C40[1]	117.9(4)	121.7(2)
C39-C40-C42	120.7(4)	121.43(19)
C40-C42-C43	178.6(5)	177.6(3)
Cp*[a]-Fe-Fe-Cp*[a]		180.0

[a] Centroid. [1]Symmetry code: -x, -y, -z.

Complex **2(PF$_6$)$_2$•2CH$_2$Cl$_2$** crystallizes in the monoclinic space group $P2_1/n$ and has an inversion center. As a consequence, the two organoiron units are crystallographically equivalent and the planes of the Cp* rings are parallel. Despite the fact that very slight geometrical differences take place between the Cp*(dppe)Fe(II)-C≡C- and [Cp*(dppe)Fe(III)-C≡C-]$^+$ series, the Cp*centroid-Fe, Fe-P, and Fe-C≡ bond lengths found in **2(PF$_6$)$_2$** are characteristic of iron(III) complexes.[68, 69] The metal-alkynyl part of the bridge is close to linearity with Fe1-C37-C38 and C37-C38-C39 angles being measured at 176.5(2) and 178.2(2)°, respectively. The presence of the alkynyl groups lowers the symmetry of the central phenyl ring. Indeed, the C39-C40 bond is somewhat longer than the C39-C41 bond (1.423(3) vs 1.406(3) Å). Within the phenyl ring, C40-C41[1] and C41-C40[1] (symmetry code: [1]:-x, -y, -z) bonds (1.394(3) Å) are the shortest ones of the ring suggesting a significant quinoidal character for the central arene group.

7. Electronic Structures of 2(PF$_6$)$_n$ (*n* = 0 - 2)

Density functional theory (DFT) calculations were carried out on both compounds ***p*-1^{n+}** and **2^{n+}** (*n* = 0 - 2) to gain further insight about the effect of the substitution of two hydrogen atoms by two ethynyl groups in modifying the electronic structures of ***p*-1^{n+}** (*n* = 0 - 2, see the Experimental Section for computational details). Note that a theoretical study of the former ones was already published a while ago at the B3LYP/LANL2DZ level of theory.[70] More specifically, for the sake of comparison with **2^{n+}**, computations were carried out again on ***p*-1^{n+}** with a larger basis set. Structural arrangements were first optimized and compared for the latter to the available X-ray data. Pertinent bond lengths and angles of the optimized molecular structures of the energetically most stable conformers found in each case are summarized in Table 3. Both for neutral and cationic species, the presence of the 2,5-ethynyl groups in **2^{n+}** hardly affects

overall the atomic distances of the rest of the molecule with respect to those computed for ***p*-1**$^{n+}$.

Upon oxidations, as expected for this kind of complex, a substantial elongation of the Fe−P, Fe−Cp* (centroid), and a contraction of Fe−C37 bond lengths is observed for both species (Table 3). Interestingly, note that computed metrical parameters for **2**$^{2+}$ with the triplet state configuration match reasonably well with the experimental data determined for **2(PF$_6$)$_2$•2CH$_2$Cl$_2$** (compare Tables 2 and 3), with the largest bond length deviations found for the Fe−C37 (< 0.045 Å).

Table 3. Pertinent computed distances (Å) and angles (°) for ***p*-1**$^{n+}$ and **2**$^{n+}$ (*n* = 0 - 2).

compd	***p*-1**	***p*-1**$^+$	***p*-1**$^{2+}$ [a]	**2**	**2**$^+$	**2**$^{2+}$ [a]
Fe1-Cp*[b]	1.750	1.761	1.781	1.753	1.765	1.783
Fe1-P1	2.283	2.310	2.368	2.285	2.314	2.375
Fe1-P2	2.275	2.296	2.338	2.277	2.299	2.338
Fe1-C37	1.897	1.843	1.896	1.892	1.842	1.898
C37-C38	1.241	1.250	1.237	1.241	1.250	1.236
C38-C39	1.425	1.403	1.425	1.419	1.401	1.422
Fe1'-Cp*[b]	1.750	1.761	1.782	1.752	1.765	1.782
Fe1'-P1	2.282	2.310	2.371	2.285	2.314	2.375
Fe1'-P2	2.276	2.297	2.338	2.279	2.299	2.339
Fe1'-C37'	1.898	1.842	1.897	1.891	1.842	1.898
C37'-C38'	1.240	1.249	1.236	1.241	1.250	1.236
C38'-C39'	1.425	1.403	1.426	1.419	1.401	1.423
Fe1...Fe1'	11.983	11.847	11.983	11.958	11.833	11.952

[a] Triplet state. [b] Centroid.

Molecular orbital (MO) diagrams of the neutral complexes ***p*-1**[70] and **2** shown and compared in Figures S1 (Supporting Indformation) are very similar. Their HOMOs have similar energy and are substantially energetically separated from the LUMOs by 3.53 and 3.40 eV, respectively (Figures 3 and 4). Their nodal properties are nearly identical, being heavily weighed on the metal-carbon bridge backbone, including the phenyl ring. As generally encountered for this kind of metal-alkynyl compound,[67] they have significant Fe−C37 antibonding and C37−C38 bonding character. On the other hand, ***p*-1** and **2** differ by their LUMOs. That of the former is strongly located on the dppe ligand tethered to the iron centers, whereas that of **2** shows a large contribution on the central ring and the 2,5-ethynyl groups with π* character. Indeed, the presence of these groups somewhat lowers its energy with respect to that of the corresponding one in ***p*-1**.

The first and second adiabatic ionization potentials (IPs) were computed for the ***p*-1** and **2** complexes. Similar values are computed for both species: 4.70 and 10.85 eV for ***p*-1**, 4.69 and 10.93 eV for **2,** for the first and second IPs, respectively.

Mulliken atomic spin densities of the mixed-valence complexes ***p*-1**$^+$ and **2**$^+$ were computed and compared in order to get some insight on the localization vs delocalization of the unpaired electron as well as some indication about the electron transfer pathway. Results show that the unpaired electron is almost evenly distributed on both iron centers and to a lesser extent on the Cβ (C38) atoms. We note that the metal contribution is somewhat higher in ***p*-1**$^+$ (0.63 e$^-$ per metal atom) that in **2**$^+$ (0.59 e$^-$ per metal atom). Corollary, the amount of spin density on the carbon bridge is more important in the latter (-0.13 e$^-$) than in the former (-0.03 e$^-$).

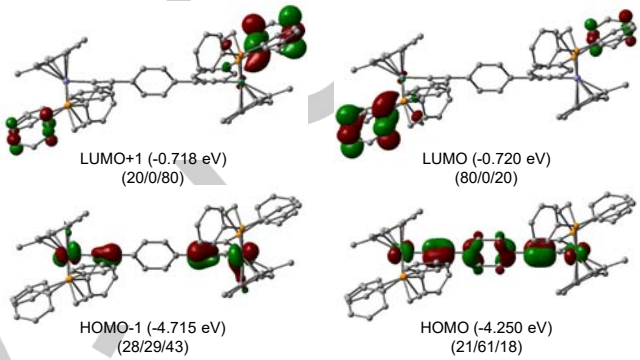

Figure 3. Plots of the HOMOs and LUMOs of ***p*-1**. The relative Fe/carbon chain/Fe percentage contributions are given in brackets. Contour values are ± 0.04 (e/bohr^3)$^{1/2}$.

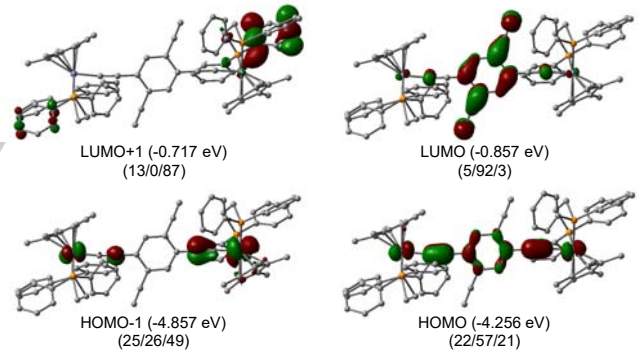

Figure 4. Plots of the HOMOs and LUMOs of **2**. The relative Fe/carbon chain/Fe percentage contributions are given in brackets. Contour values are ± 0.04 (e/bohr^3)$^{1/2}$.

Time-dependent density functional theory (TD-DFT) calculations were carried out on these monocationic species. Results indicate that in the NIR energy range, one relatively weak band is computed for ***p*-1**$^+$ and **2**$^+$. Each band can be decomposed into two sub-bands at 6380 cm^{-1} (0.791 eV) and 6533 cm^{-1} (0.810 eV) for ***p*-1**$^+$**,** and at 6275 cm^{-1} (0.778 eV) and 6299 cm^{-1} (0.781 eV) for **2**$^+$. A glance at the main electronic transitions responsible for these absorption bands reveals for both species an important electron transfer from the ethynyl groups to the iron centers, i.e., ligand-to-metal charge (LMCT) rather than intervalence charge transfer (IVCT).

For the dicationic species ***p*-1**$^{2+}$ and **2**$^{2+}$, the energies of the different spin states, i.e., the closed-shell singlet (S, diamagnetic state), the open-shell triplet (T, ferromagnetic state) and the broken-symmetry (BS, diamagnetic state) configurations were computed. For both molecules**,** the diamagnetic state (S) is computed to be energetically largely disfavored (by more than 1.40 eV) with respect to the magnetic states. On the other hand, the ferro- (T) and antiferromagnetic spin (BS) states are very close in energy with the latter very slightly preferred (0.003 eV (24 cm^{-1}) and 0.013 eV (103 cm^{-1}) for ***p*-1**$^{2+}$ and **2**$^{2+}$, respectively) for the most stable structures. It can be concluded that the addition of ethynyl groups on the phenyl ring in compound **2**$^{2+}$ leads to some increasing of the antiferromagnetic coupling. Energies of both spin states (computed at 0 K) are sufficiently close to consider thermal population of conformers that may differ through rotation for instance of one half-sandwich fragment relative to the phenyl ring.

A conformational study was then performed on both dicationic complexes ***p*-1**$^{2+}$ and **2**$^{2+}$. A series of different rotamers corresponding to complexes where the Cp*(centroid)−Fe−Fe−Cp*(centroid) dihedral angle ω was varied, were fully optimized in both singlet and triplet state configurations. The main optimized data obtained for these different conformations are given in Table S2 (Supporting Information). Note that some highly sterically hindered rotamers could not be computed. Interestingly, the potential energy curve for the unsubstituted dication ***p*-1**$^{2+}$ remains rather flat indicating almost free rotation. Total energies of the ferromagnetic and antiferromagnetic states remain similar with the latter always energetically favored (by ca. 20-25 cm^{-1}). For the di-ethynyl substituted species **2**$^{2+}$, a more hilly potential energy curve is computed with energy differences up to 100 cm^{-1} between rotamers but also always in favor of the antiferromagnetic state. Such small differences between low spin and high spins configurations indicate that if the former constitutes the ground state configuration at low temperature, the latter might be easily accessible as the temperature increases (vide infra).

8. ^{57}Fe Mössbauer Spectroscopy for 2(PF$_6$)$_n$ (*n* = 0 - 2)

The Mössbauer spectra of the three complexes **2(PF$_6$)$_n$** (*n* = 0 - 2) were run at 80 K and least-squares fitted with Lorentzian line shapes.[71] The isomeric shift (IS) and the quadrupole splitting (QS) parameters are given in Table 4 with the data previously reported for the complexes ***p*-1(PF$_6$)$_n$** (*n* = 0 - 2) for comparison. The spectrum of the neutral bis-iron(II) complex **2** shows a single doublet with IS and QS parameters in line with values previously reported for iron(II) complexes of the same series.[7, 8] In particular, the data found for the analogous derivative ***p*-1** are very close but slightly larger indicating that the C≡CH fragments act somewhat as electron withdrawing groups with respect to the iron nuclei. Despite the fact that the iron nuclei should be less electron rich in **2** than in ***p*-1**, oxidation of the former is slightly easier by 0.01 V (Table 1).

The spectrum of the dication **2(PF$_6$)$_2$** also displays a single doublet with QS and IS parameters close to the values reported for ***p*-1(PF$_6$)$_2$** and in the typical range of data expected for low spin d^5 Fe(III) centers.[8, 66, 72] These bisiron(III) compounds contain two unpaired electrons giving rise to a mixture of molecules in the singlet state (*S* = 0, antiferromagnetic state) and in the triplet state (*S* = 1, ferromagnetic state). Experimental data and theoretical calculations on ***p*-1**$^{2+}$ showed that the singlet state is the ground state and the energies for the antiferromagnetic and ferromagnetic states are close enough to allow thermal population of both states at 80 K (see Sections 7 and 11). The observation of a single doublet for the spectra of both ***p*-1(PF$_6$)$_2$** and **2(PF$_6$)$_2$** is consistent with a fast exchange between the two spin states on the Mössbauer timescale as previously suggested for other related compounds.[73] It can be mentioned that for the bisiron(III) [Cp*(dppe)FeC(OMe)CHCHC(OMe)Fe(dppe)Cp*](PF$_6$)$_2$ complex, two resolved doublets were observed for the triplet state (QS = 0.8 mm/s) and the singlet state (QS = 1.1 mm/s).[74]

Table 4. Mössbauer parameters for complexes ***p*-1(PF$_6$)$_n$**, and **2(PF$_6$)$_n$** (*n* = 0-2).

compd	QS (IS) mm/s vs Fe, 80 K			
	Fe(II)	Fe(averaged)	Fe(III)	relative areas (%)
***p*-1**	2.02 (0.26)			100
***p*-1(PF$_6$)**	1.96 (0.25)	1.11 (0.20)	0.71 (0.25)	14/72/14
***p*-1(PF$_6$)$_2$**			0.91 (0.24)	100
2	1.97 (0.25)			100
2(PF$_6$)	1.90 (0.25)	1.79 (0.16)	0.97 (0.21)	37/26/37
2(PF$_6$)$_2$			0.88 (0.21)	100

Interestingly, the Mössbauer spectra of polycrystalline samples of ***p*-1(PF$_6$)** was found consistent with a solid solution containing both the mixed-valence (MV, Fe^{II}-Fe^{III} valence trapped) form, and a detrapped component (Fe (averaged), the proportions of which were found to vary from sample to sample with recrystallization procedures. This behavior has been attributed to variations in local environment of the molecule brought by differences in delocalization of the odd-electron into π-orbitals of the bridging ligand associated with rotations of the bridge and the metal termini.[60]

The ^{57}Fe Mössbauer spectrum of the monocationic complex **2(PF$_6$)** displays three distinct doublets with relative spectral absorption areas in the 37/26/37 ratio (Figure 5). The two doublets with equivalent surface areas are characterized with IS and QS parameters close to the values found for the homovalent parent compounds.[60] They can be assigned to a trapped MV compound with exchange rate constant $k_e < 10^6$ s^{-1}. The intermediate doublet corresponds to molecules in which the electron exchange rate is much faster ($k_e > 10^9$ s^{-1}).

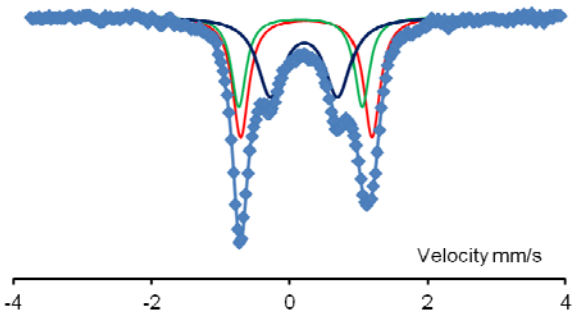

Figure 5. ^{57}Fe Mössbauer spectrum of **2(PF$_6$)** at 80 K.

Comparison of the Mössbauer parameters found for the cationic complexes ***p*-1(PF$_6$)** and **2(PF$_6$)** shows that in both cases, the samples contain trapped and detrapped components with a relative ratio depending on the mode of precipitation of the solid materials. In the case of the trapped forms, the Mössbauer parameters are consistent with similar electronic structures for the two cationic complexes.

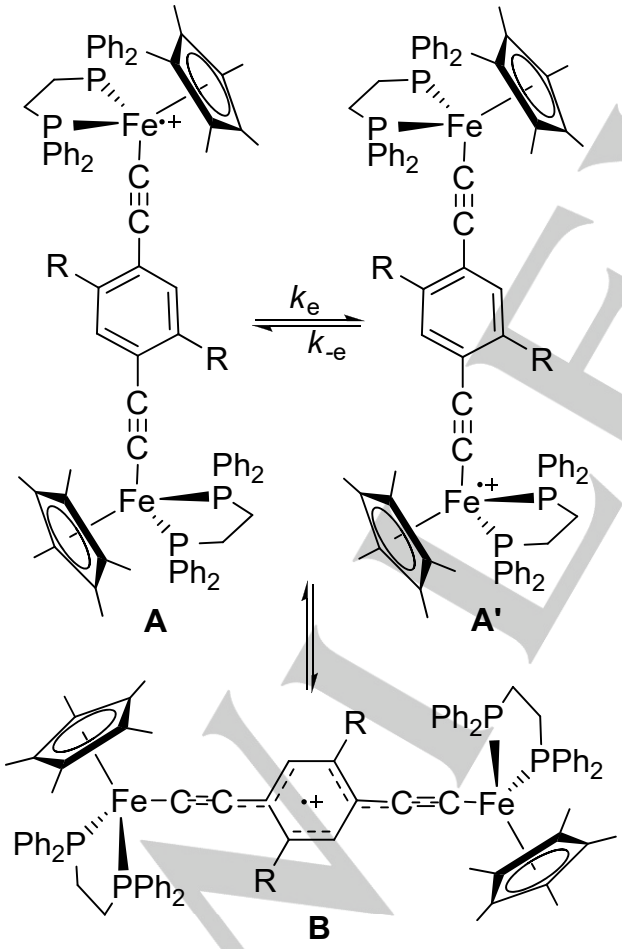

Scheme 4. Schematic Representation of the bridge and mixed-valence states. For R = H, the population of the bridge-state was not detected. For R = C≡CH, the population of the bridge-state is 1/4 in the solid state.

In the case of the detrapped systems, the QS parameters are significantly different for ***p*-1(PF$_6$)** and **2(PF$_6$)**. While the QS value (QS = 1.11 mm/s) found for ***p*-1(PF$_6$)** is somewhat smaller than the average value of the two homovalent complexes ***p*-1** and ***p*-1(PF$_6$)$_2$** (QS_{av} = 1.31 mm/s) in accord with a formal oxidation state of the iron centers slightly above 2.5 probably associated with the development of a partial negative charge on the carbon bridge, a completely different situation is observed in the case of **2(PF$_6$)**.[60] Indeed, for this latter compound the QS parameter (1.79 mm/s) is much larger than the averaged value (QS_{av} = 1.39 mm/s), indicating a formal oxidation state of the iron nuclei only slightly above 2. Consequently, an important contribution of the carbon-rich bridge to the delocalization of the positive charge and the spin density is expected. The large difference in the QS values for the detrapped mixed-valence complexes ***p*-1(PF$_6$)** and **2(PF$_6$)** constitutes a clear experimental evidence of the effect of the two C≡CH fragments on the electronic properties of these compounds. The Mössbauer data show that the presence of the alkynyl substituents favors the trapped Fe(II)-Fe(III) MV form with respect to the detrapped one. In addition, in the minor detrapped form, the positive charge is mainly bridge-centered in **2(PF$_6$)**, while it was found iron-centered in ***p*-1(PF$_6$)**. This experimental result is consistent with DFT calculations which indicate that the amount of spin density on the carbon bridge is greater in **2$^+$** than in ***p*-1$^+$**.

Simultaneous observation of an iron localized and delocalized mixed valence compound is far to be unprecedented. In particular, a similar behavior was also found in the case of the octatetraynediyl-bridged bis-iron complex [Cp*(dppe)Fe-(C≡C)$_4$-Fe(dppe)Cp*](PF$_6$).[75] Many years ago, a similar behavior was also reported by Hendrickson for the 1',1'''-dibenzylbiferrocenium triiodide monocation.[76-79] Indeed, a polycrystalline sample can be regarded as a solid solution containing population of various conformers of the same molecules. In the case of complex ***p*-1(PF$_6$)** the relative conformation of the bridging ligand and the metal centers switches the magnitude of the electronic coupling between the metal centers yielding population of trapped and detrapped mixed-valence species at the spectroscopic time scale. The QS parameters of the detrapped species are close to the averaged values found for the trapped mixed-valence form and therefore the electronic structures of the trapped and detrapped compounds are very similar. Finally, they differ between each other essentially by the rate of the intramolecular electron transfer as shown in Scheme 5 for mesomers **A** and **A'**.[75] In the case of the cationic complex **2(PF$_6$)**, the relative orientation of the metal termini and bridge not only modify the rate of the intramolecular electron transfer at the Mössbauer time scale, but also switches the positive charge density from the metal atoms to the carbon bridge (redox isomer **B**, Scheme 4). To our knowledge, the simultaneous observation of populations of mixed-valence and bridge-oxidized states by Mössbauer spectroscopy for organometallic radicals composed of two redox-active termini connected by a carbon rich ligand is unprecedented. However, a combination of UV-vis-NIR and IR spectroscopies on diruthenium radical cations featuring diethynylaromatic bridging ligands have also established that bridge-centered radical cations and mixed-valence species can

both be present in the fluid solution.[80] We can also mention that some of us found that the intramolecular electron transfer is bridge-mediated in the case of the radical cation [3,5-{Cp*(dppe)Fe-C≡C-}$_2$(NC$_4$H$_3$)](PF$_6$).[81]

9. Glass ESR Spectroscopy of 2(PF$_6$)$_n$ (*n* = 1, 2).

The X-band ESR spectra of **2(PF$_6$)** and **2(PF$_6$)$_2$** were recorded at 66 K in a rigid glass (CH_2Cl_2). The *g* values extracted from the spectra are collected in Table 5. The sample of the dicationic complex **2(PF$_6$)$_2$** is ESR silent. In the case of complex ***p*-1(PF$_6$)$_2$** a very weak signal has been observed.[60] As the antiferromagnetic ground state is ESR silent, the signal comes from the triplet excited state. Consequently, it can be assumed that the singlet to triplet energy gap is probably larger in **2(PF$_6$)$_2$** than in ***p*-1(PF$_6$)$_2$** (see Section 13).

The spectrum of the radical cation **2(PF$_6$)** shows a signal with three main components characteristic of pseudo-octahedral geometry of the d^5 low spin iron(III) complexes. The values of the three components of the *g* tensor are in the range generally found for this type of complex and rather close to those reported for ***p*-1(PF$_6$)**.[8, 60] The g_{iso} tensors are similar for the two complexes ***p*-1(PF$_6$)** and **2(PF$_6$)** in accord with a very similar contribution of the metal centers in the description of the SOMOs.

Table 5. ESR Parameters for ***p*-1(PF$_6$)$_n$** and **2(PF$_6$)$_n$** (*n* = 1, 2) at 66 K

compd	g_{iso}	g_1	g_2	g_3	Δg	ref
***p*-1(PF$_6$)**	2.091	2.199	2.043	2.031	0.168	[60]
***p*-1(PF$_6$)$_2$**		2.032 (ΔHpp ca. 160 G)				[60]
2(PF$_6$) [a]	2.083	2.2085	2.0392	2.0020	0.2065	[b]
2(PF$_6$)$_2$		ESR silent				[b]

[a] Line broadening: S1 = 50 G, S2 = 15 G, S3 = 15 G. [b] This work

The key feature here is the anisotropy ($\Delta g = g_1 - g_3$) significantly larger for **2(PF$_6$)** than for ***p*-1(PF$_6$)**. Indeed, it has been observed for several mixed-valence series including the Cp*(dppe)Fe-C≡C-L-C≡C-Fe(dppe)Cp*]$^+$ series that the anisotropy of the ESR signal decreases as the rate of the intramolecular electron transfer increases.[8, 75, 82] Consequently, the comparison of the Δg anisotropy of these two complexes indicates that the intramolecular rate of electron transfer between the redox centers should be smaller in **2(PF$_6$)** than in ***p*-1(PF$_6$)**.

10. IR Spectroscopy of 2(PF$_6$)$_n$ (*n* = 0 - 2). The IR spectra were run for powdered samples of **2(PF$_6$)$_n$** (*n* = 0 - 2, Figure 6). The frequencies of $\nu_{FeC\equiv C}$ and ν_{aryl} bands for **2(PF$_6$)$_n$** are collected in Table 6 for the three redox states (*n* = 0 - 2) and the energy of the corresponding bands for ***p*-1(PF$_6$)$_n$** are recalled for comparison. It is clear from Figure 6 that the intensity of the $\nu_{C\equiv C}$ bands decreases as the positive charge increases. The vibration mode corresponding to the C≡CH triple bond is clearly observed at 2100 cm^{-1} in the spectrum of the neutral complex. However, they are so weak in the spectra of the mono- and dicationic species that their observation was not possible for all samples. When they can be observed, their energy is almost independent of the number of charges on the molecule in the accuracy of the measurements (± 2 cm^{-1}).

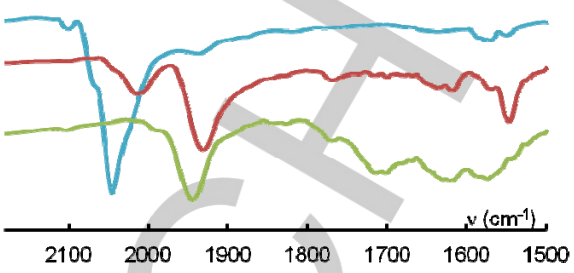

Figure 6. IR spectra in Nujol (KBr plates) for **2(PF$_6$)$_n$** (from top to bottom: *n* = 0, 1, 2 for powdered samples, and *n* = 2 for crushed single crystals).

The IR spectrum of **2** exhibits one strong band at 2046 cm^{-1}. This band corresponds to the antisymmetric mode of vibration of the Fe(II)-C≡C triple bond. This band can also be observed in the IR spectrum of ***p*-1** at 2051 cm^{-1}.[60, 83] The IR spectra of the Fe(III)-Fe(III) dications ***p*-1(PF$_6$)$_2$** and **2(PF$_6$)$_2$** display also one band of medium intensity corresponding to the antisymmetric $\nu_{C\equiv C}$ mode of vibration at 1987 or 1947 cm^{-1}, respectively. These frequencies fit well with the data collected for the Cp*(dppe)Fe(II)-C≡C and Cp*(dppe)Fe(III)-C≡C stretching modes which are generally observed in the 1910-2040 cm^{-1} range.[8, 84] Interestingly, a comparison of the IR spectra of ***p*-1(PF$_6$)$_2$** and **2(PF$_6$)$_2$** shows a decrease by ca. 35 cm^{-1} of the energy of the $\nu_{FeC\equiv C}$ band in the latter complex. It clearly appears that the presence of the terminal alkyne on the central phenyl ring contributes to decrease the FeC≡C bond order. One of the consequence of this effect should be the stabilization of the diamagnetic state with respect to the triplet excited state for the diradical **2(PF$_6$)$_2$**.

Table 6. Experimental IR $\nu_{Fe-C\equiv C}$ and ν_{aryl} (cm^{-1}) bands for **2(PF$_6$)$_n$** and the closely related complex ***p*-1(PF$_6$)$_n$** (*n* = 0 - 2).

compd	*n* = 0	*n* = 1	*n* = 2	ref
***p*-1(PF$_6$)$_n$** [a]	2051 (s)	2016 (m) 1934 (s) 1568 (m) [c]	1987 (m)	[83]
2(PF$_6$)$_n$ [b]	2046 (s)	2020 (m) 1936 (s) 1550 (m)	1947 (m)	[c]
2(PF$_6$)$_n$ [a]		2013 (w) 1935 (s) 1550 (m)		[c]

[a] In CH_2Cl_2. [b] Powder, Nujol mull, KBr plates. [c] This work.

The IR spectrum of the monocationic complex **2(PF$_6$)** is essentially characterized by two bands at 2020 and 1936 cm^{-1} which can be assigned to the Fe(II)C≡C and Fe(III)C≡C bond stretching modes, respectively. The spectrum of the related complex ***p*-1(PF$_6$)** is quite similar with two bands at 2016 and 1934 cm^{-1}.[83] The relative intensities of the two bands remain

constant and can be assigned to a localized mixed-valence state. The IR and the Mössbauer data indicate that the trapped MV state for ***p*-1(PF$_6$)** and **2(PF$_6$)** should have similar electronic structures. This is also fully supported by quantum chemistry calculations.

Beside the $\nu_{FeC\equiv C}$ stretching modes, the IR spectrum of **2(PF$_6$)** also displays a band of medium intensity at 1550 cm^{-1}. This band, which does not exist in the spectra of the related homovalent relatives, can be assigned to a $\nu_{C=C}$ mode of vibration of the aromatic portion of the bridge. Similar $\nu_{C=C}$ bands were also observed in the IR spectra of [Cp*(dppe)RuC≡C-1,4-C$_6$H$_4$-C≡CRu(dppe)Cp*](PF$_6$), the ruthenium analog of ***p*-1(PF$_6$)**.[80] This feature was found to be consistent with the end-to-end dipole across the molecule in the localized mixed-valence state.[80] The spectroscopic signature of the delocalized isomer was not identified in the IR spectrum of **2(PF$_6$)**.

11. UV-Vis Spectroscopy for 2(PF$_6$)$_n$ (*n* = 0 - 2)

The UV-vis spectra of complexes **2(PF$_6$)$_n$** (*n* = 1, 2) were recorded between 350 and 800 nm at 20 °C in CH_2Cl_2. The characteristic data are collected in Table 7, along with those of ***p*-1(PF$_6$)$_n$**. The bands around 420, and 509 nm found in the spectrum of **2** correspond to metal-to-ligand charge-transfer (MLCT) transitions.[85] They are red-shifted to 460, 595 nm in **2(PF$_6$)**. In accord with a bridge delocalized ground state in **2(PF$_6$)**, a smaller red-shift was reported for the reference complex ***p*-1(PF$_6$)**.[60] A third band observed in the spectrum of **2(PF$_6$)** at 634 nm can be tentatively assigned to a ligand-to-metal charge transfer (LMCT). The bands at 605, 690, 780 nm found in the spectrum of **2(PF$_6$)$_2$** can be safely ascribed to LMCT transitions.[69]

Table 7. Absorptions in the visible for complexes ***p*-1(PF$_6$)$_n$** and **2(PF$_6$)$_n$** in CH_2Cl_2 at 20 °C.

compd	absorptions λ (nm) (ε x 10^{-3} (M^{-1} cm^{-1}))	Ref
***p*-1**	411 (25.4), 525 (3.4)	[83]
***p*-1(PF$_6$)**	424 (8.7), 547 (17.0), 702 (7.6)	[83]
***p*-1(PF$_6$)$_2$**	420 (8.0), 619 (sh 5.4), 702 (42.8), 769 (sh 7.1)	[83]
2 [b]	420 (20.0), 509 (15.2),	[a]
2(PF$_6$)	460 (6.0), 595 (sh 8.9), 634 (11.2),	[a]
2(PF$_6$)$_2$	440 (9.6), 490 (7.6), 605 (6.6), 690 (22.6), 780 (5.5)	[a]

[a] This work. [b] Due to the bad solubility of **2**, the spectrum is very noisy and the values of ε are uncertain.

12. NIR Spectroscopy for 2(PF$_6$)

The IR and Mössbauer spectra of ***p*-1(PF$_6$)** and **2(PF$_6$)** are consistent with a population of trapped FeII/FeIII MV state in polycrystalline samples and in solution (Robin-and-Day Class-II compound).[86] In addition, at a much slower time scale, Mössbauer spectroscopy allowed the observation of detrapped forms for both monocationic derivatives. However, the electronic structures are different in these two cases. A strong metallic character was found for ***p*-1(PF$_6$)** while a dominant bridge character characterizes **2(PF$_6$)**. As a consequence, the detrapped redox isomer of **2(PF$_6$)** cannot be regarded as a mixed valence derivative since the charge is essentially localized on the bridge, which shows a "redox-non innocent behavior.[80, 87-90] It is anticipated that the NIR spectra of ***p*-1(PF$_6$)** and **2(PF$_6$)** should reflect the different electronic properties of these compounds.

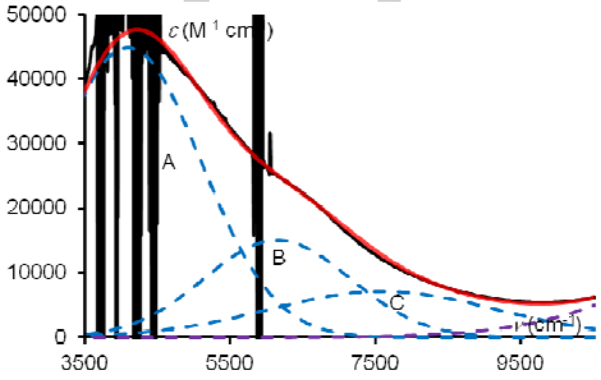

Figure 7. NIR spectrum of **2(PF$_6$)** in CH_2Cl_2 and proposed deconvolution.

The NIR spectrum of ***p*-1(PF$_6$)** previously reported is characterized by a very intense intervalence charge-transfer band (IVCT) with a cutoff on the low energy side. A strong electronic coupling (ca. 1700 cm^{-1}) was derived from the band shape analysis for this MV complex that was found to be a Class-II MV complex, close to the border between Class II and Class III.[83] The NIR spectrum of the monocationic complex **2(PF$_6$)** also displays a broad absorption with a complex shape (Figure 7). However, the experimental spectrum is more than four times more intense than that of ***p*-1(PF$_6$)** (ε = 50 000 M^{-1} cm^{-1}) suggesting that different electronic transitions should be involved.

The envelope of this broad absorption can be deconvoluted into the sum of three Gaussian-shaped sub-bands (A, B, C) in the 3500 - 10 000 cm^{-1} range. The characteristic parameters of the three Gaussian components (ν_{max}, ε_{max}, and $\Delta\nu_{1/2}^{exp}$) are collected in Table 8. In contrast with many related monocationic binuclear systems with the general structure [Cp*(dppe)Fe-*B*-Fe(dppe)Cp*]$^+$ including ***p*-1(PF$_6$)**,[7, 8, 83, 91] a good fit cannot be obtained with three sub-bands with the same band width at half-height. Indeed, bands A and B are much narrower than band C indicating that they should have a different origin.

In the two-state model approximation, the NIR spectra of Class-II MV complexes are expected to be solvent sensitive.[92, 93] This feature has been observed for all of the monocationic models containing two Cp*(dppe)FeC≡C units linked by a carbon-rich bridge with only two exceptions where the mediating bridges are 1,3-phenyl and 3,5-pyridine.[81] For these MV compounds, it was

found that the NIR bands do not correspond to IVCT but rather to LMCT.[81]

Table 8. NIR data for **2(PF$_6$)** in CH_2Cl_2 and CH_3CN at 25 °C, and the related compound ***p*-1(PF$_6$)**.

compd (solvent)	ν_{max} (cm^{-1})	ε (dm^3 mol^{-1} cm^{-1})	$\Delta\nu_{1/2}$exp (cm^{-1})	$\Delta\nu_{1/2}$calcd (cm^{-1})	ref
***p*-1(PF$_6$)**	4000	12700	2120	3040	[83]
(CH_2Cl_2)	6500	3400	2110	3880	
	9000	600	2110	4560	
2(PF$_6$)	4100	45000	1420		[a]
(CH_2Cl_2)	6150	15000	1420		
	7600	7100	2200	4190	
2(PF$_6$)	4120	15000	1400		[a]S
(CH_3CN)	6280	7400	1400		
	8300	1600	2100	4380	

[a] This work.

To specify the origin of the absorption bands, the spectrum of **2(PF$_6$)** was also run in acetonitrile and deconvoluted. The key parameters of the three Gaussian components are given in Table 8. The energy of bands A and B are almost independent of the polarity of the solvent. With respect to the spectrum recorded in CH_2Cl_2, the peak positions of bands A and B are only slightly blue-shifted by 20 and 130 cm^{-1}, respectively. As a result, it can safely be concluded that the bands A and B cannot be assigned to IVCT. Very probably, they correspond to LMCT, in accord with an intramolecular electron transfer involving the bridge in the ground state. This is supported by the TD-DFT calculations which show two sub-bands involving LMCT rather than IVCT (vide supra).

In contrast, the energy of band C located at higher energy is more sensitive to the nature of the solvent. A blue shift of 700 cm^{-1} is observed when CH_2Cl_2 is replaced by CH_3CN. This is in line with previous observation made for Class-II MV complexes of the same series.[73] We can conclude that the low-energy band C found in the NIR spectrum of **2(PF$_6$)** corresponds to an IVCT. This band constitutes the NIR signature of the trapped MV component. As this MV complex belong to Class II, the two-level Hush model applies. In particular, the full width of the band at half height should obey eq 1 and the electronic coupling can be calculated with eq 2.[93]

$$(\Delta\nu_{1/2})_{calc} = (2310 \times \nu_{max})_{1/2} \quad (1)$$

$$H_{ab} = (2.06 \times 10^{-2}/d_{ab})(\varepsilon_{max} \times \nu_{max} \times \Delta\nu_{1/2})^{1/2} \quad (2)$$

The calculated band width is almost twice as large as the experimental value indicating that the metal-metal interaction is rather strong and that the condition of the weak interaction limit for the application of Hush model is not completely fulfilled.[93] The electronic coupling derived from eq 2 for **2(PF$_6$)** (using the Fe-Fe distance determined by X-ray analysis for the closely related compound **2(PF$_6$)$_2$** (H_{ab} = 601 cm^{-1}) is apparently smaller than the value found for ***p*-1(PF$_6$)** (H_{ab} = 1700 cm^{-1}). However, if one assumes that solutions of **2(PF$_6$)** also contain a trapped component, this value is probably underestimated. Therefore, these data must be compared with caution, but nevertheless it seems that the presence of the two ethynyl fragments on the aromatic ring weakens the metal-metal interaction. Note that ESR and NIR spectroscopic analyses lead to the same conclusion, independently. However, it is also important to keep in mind that according to the TD-DFT results (see above), similar conformers of ***p*-1(PF$_6$)** and **2(PF$_6$)** show NIR bands comparable energy. Therefore, most probably, one compares H_{ab} for some conformers of **2(PF$_6$)** with that of a different type of conformers of ***p*-1(PF$_6$)**.

13. ^{1}H NMR and Magnetic Behavior of 2(PF$_6$)$_2$

The magnetic coupling defined as the energy difference between the singlet and triplet states (ΔE_{ST}, see Section 7) in the dicationic Fe(III)-Fe(III) complex is also modified by the introduction of alkynyl substituents at the 2,5-positions of the central arene of the bridge. It is known that the low-spin mono- and dinuclear complexes of the Cp*(dppe)Fe(III) series are generally both NMR active in the range of temperature where the usual solvents are liquid (ca. 190 - 300 K) and ESR active at low temperature (66 K and below).[94] The ^{1}H NMR spectrum of **2(PF$_6$)$_2$** was recorded at 298 K in CD_2Cl_2 (Figure 8). Similarly to the related complex ***p*-1(PF$_6$)$_2$**, the spectrum of **2(PF$_6$)$_2$** displays a single set of paramagnetically shifted signals in accord with a fast interconversion between the singlet and triplet states with respect to the NMR time scale. The assignment of the resonances as shown in Figure 8 was achieved by analogy with that reported for ***p*-1(PF$_6$)$_2$**.[95]

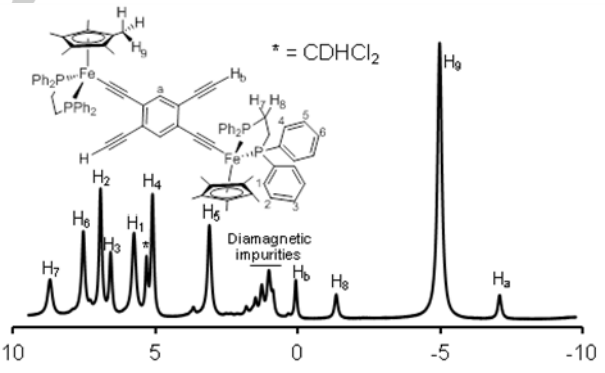

Figure 8. ^{1}H NMR spectrum (CD_2Cl_2, 298 K) of **2(PF$_6$)$_2$**.

The nonambiguous assignment of the latter spectrum was proved possible by using ^{1}H - ^{1}H polarization transfer.[95] Most of the resonances are observed at similar chemical shifts for both compounds, except that of the proton directly bound to the central aromatic ring H_a (see right of Figure 8). In this particular case, H_a is observed at δ -7.08 for **2(PF$_6$)$_2$**, while it was found at δ -4.5 in the case of ***p*-1(PF$_6$)$_2$**.[95] This shift suggests that the

spin density on the central phenyl ring should be larger in **2(PF$_6$)$_2$** than in ***p*-1(PF$_6$)$_2$**.

The magnetic exchange interactions between [Cp*(dppe)Fe]$^+$ termini in bimetallic and trimetallic derivatives were early recognized and subject of various studies on powdered samples.[95-99] It is an important factor which impacts the redox potentials and the comproportionation constants in these complexes.[100] The variation of the magnetic susceptibility with temperature on powderous samples for these families of complexes is often intriguing and varies from sample to sample, reflecting the importance of the molecular conformation on the magnetic properties. Measurements on fluid solution by NMR have proven to give much more reproducible results.[18, 95, 99]

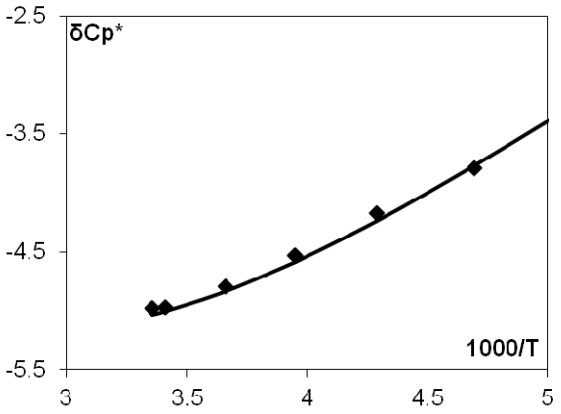

Figure 9. Plot of the observed (squares) vs calculated (solid line) temperature dependence of the ^{1}H chemical shift of δCp* for **2(PF$_6$)$_2$**.

For paramagnetic compounds, the observed NMR chemical isotropic shift may arise from contact and/or dipolar interactions.[101] It has been established for the [Cp*(dppe)Fe]$^+$ spin carriers that the isotropic shift is essentially contact in origin.[18, 97] In the consequence, the Curie law is obeyed and a linear relationship is observed for δ vs 1/*T* as long as the singlet/triplet ratio remains constant. This is the case when the ground state and the excited state are close in energy. Indeed, in the range of temperatures accessible for fluid solution (ca. 190 - 300 K) the states are statistically populated. However, for compounds in which the singlet-to-triplet energy gaps are larger, population of the ground state can significantly increase as the temperature decreases, thereby inducing deviations from Curie law. The variation of the magnetic susceptibility is given by the Bleaney-Bowers equation (eq 3), which is derived from the van Vleck equation:[102, 103]

$$\chi = C/T\,[3 + \exp(-J/kT)] \quad (3)$$

Variable-temperature ^{1}H NMR spectra were recorded for **2(PF$_6$)$_2$** from 298 to 193 K. It was observed that all the resonances move toward the positions usually found for diamagnetic compounds when the temperature decreases, establishing that the singlet state is the ground state. As previously observed for mononuclear and dinuclear complexes in the Cp*(dppe)Fe series, the presence of unpaired electrons predominantly affects the chemical shifts of the methyl groups of the Cp* ligands.[18, 94, 99] This is also true in the case of **2(PF$_6$)$_2$**. The experimental plot of the variation of the chemical shift of the proton on the Cp* ligands (δ_{Cp^*}) against 1/*T* is shown in Figure 9. The solid line fitting the experimental data shown as squares correspond to the best fit of coupling parameter *J* obtained by using eq 3. The experimental *J* values are negative indicating that both dications are antiferromagnetically coupled and decrease from *J* = -340 cm^{-1} for ***p*-1(PF$_6$)$_2$** to *J* = -530 cm^{-1} for **2(PF$_6$)$_2$**. Substitution of two H atoms by ethynyl C≡CH fragments in the aromatic ring at the 2 and 5 positions of the bridge increases the gap by ca. 200 cm^{-1}. Computational results discussed in Section 7 are in full agreement.

Conclusions

A straightforward procedure was found to prepare the bis(iron) acetylide complex [1,4-{Cp*(dppe)Fe-C≡C-}$_2$-2,5-(C≡CH)$_2$-C$_6$H$_2$] (**2**) from 1,2,4,5-tetraethynylbenzene and two equiv of Cp*(dppe)FeCl via the bis(iron-vinylidene) complex [1,4-{Cp*(dppe)Fe=C=CH}$_2$-2,5-(C≡CH)$_2$-C$_6$H$_2$](PF$_6$)$_2$ (**[2-2H](PF$_6$)$_2$**). The reaction is highly chemo- and regioselective and the target complex was isolated in good yield. The related mono- and dicationic complexes **2(PF$_6$)$_n$** (*n* = 1, 2) were also prepared in high yields, isolated in pure forms, and characterized by various means including an X-ray diffraction analysis for **2(PF$_6$)$_2$**.

The experimental and theoretical study of the complexes **2(PF$_6$)$_n$** (*n* = 0 - 2) and comparison with the unsubstituted reference derivatives [1,4-{Cp*(dppe)FeC≡C}$_2$-C$_6$H$_4$](PF$_6$)$_n$, ***p*-1(PF$_6$)$_n$** (*n* = 0 - 2), have provided some information on how the presence of ethynyl groups located at the 2,5 positions of the central aromatic ring can affect the chemical, electronic, and magnetic properties of the latter. Indeed, deprotonation of the bis(iron-vinylidene) complexes [1,4-{Cp*(dppe)Fe=C=CH}$_2$-2,5-(C≡CH)$_2$-C$_6$H$_2$]$^{2+}$ leading to the formation of **2** is particularly difficult. These ethynyl groups play an important role on the electronic properties of the radical cation. Solutions of the radical cations ***p*-1(PF$_6$)** and **2(PF$_6$)** contain both valence trapped and valence detrapped species. It turns out that the simultaneous thermal population of these two states is related to several factors, including the orientation of the phenyl ring of the bridge with respect to the iron alkynyl termini. In both cases, the trapped MV form is characterized by a strong localization of the spin and charge on the iron termini. However, the presence of the terminal ethynyl moieties on the aromatic ring of the bridge weakens the metal-metal interaction. As a consequence, the electronic coupling H_{ab} is decreased. Interestingly, the major difference deals with the detrapped redox isomers. While it was found for the reference complex ***p*-1(PF$_6$)** that the one-positive charge and unpaired spin density show predominantly a metal character in the detrapped form, complex **2(PF$_6$)** exhibits rather characteristics of a bridge-oxidized radical. Comparison of these characteristics with those of the ruthenium analogue [1,4-{Cp*(dppe)Ru-C≡C}$_2$-C$_6$H$_4$](PF$_6$)[80] indicates that the introduction of two terminal alkynes at the 2,5-positions of the aromatic ring of the bridging ligand has a comparable effect as the

replacement of the two iron centers by two ruthenium nuclei in ***p*-1(PF$_6$)**. The electronic structure of the dicationic species is also modified by the terminal ethynyl substituents. The energy difference between the singlet ground state and the triplet excited state increases substantially upon substitution. This stronger antiferromagnetic coupling likely results from a significant contribution of the bridge π-orbitals.

For the future design of new derivatives containing four metal centers, the fact that the 2,5-ethynyl groups on the central aromatic ring do not contribute to the description of the HOMO constitutes a key feature. In particular, it can be expected that partial localization of the charge and spin and electron transfer between trans-disposed Cp*(dppe)Fe entities along the molecular 1,4- and 2,5-axes would be favored with respect to a full delocalization of the unpaired electrons on the whole molecule. Work to confirm this assumption is in progress in our laboratory.[58]

Experimental Section

Experimental Details: Manipulations of air-sensitive compounds were performed under an argon atmosphere using standard Schlenk techniques. Tetrahydrofuran (THF), toluene and pentane were dried and deoxygenated by distillation from sodium/benzophenone ketyl. Dichloromethane was distilled under argon from P_2O_5 and then from Na_2CO_3. Methanol was distilled over dried magnesium turnings. Compounds Cp*(dppe)FeCl (**3**)[94] and 1,2,4,5-tetra-(trimethylsilyl-ethynyl)benzene[104] were prepared according to published procedures. Other chemicals were purchased from commercial sources and used without further purification. Infrared spectra were obtained as KBr pellets with a Bruker IFS28 FTIR infrared spectrophotometer (4000-400 cm^{-1}). Near-IR and UV-visible spectra were recorded as CH_2Cl_2 solutions, using a 1 cm long quartz cell on a Cary 5000 spectrophotometer. ^{1}H, ^{13}C, and ^{31}P NMR spectra were acquired on a Bruker AVIII 400 multinuclear NMR spectrometer at ambient temperature, unless otherwise noted. Chemical shifts are reported in parts per million (δ) relative to tetramethylsilane (TMS), using the residual solvent resonances as internal references for ^{1}H and ^{13}C and external H_3PO_4 (0.0 ppm) for ^{31}P NMR spectra. Coupling constants (*J*) are reported in Hertz (Hz). High-resolution mass spectra (HRMS) were recorded on a high-resolution Waters Q-Tof 2 spectrometer operating in the ESI$^+$ mode. Cyclic voltammograms were recorded in dry CH_2Cl_2 solutions containing 0.1 M [Bu$^n_4$N](PF$_6$) as supporting electrolyte, purged with argon and maintained under argon atmosphere, using a EG&G-PAR model 362 potentiostat/galvanostat. The working electrode was a Pt disk, the counter electrode a Pt wire and the reference electrode a saturated calomel electrode. The ferrocene/ferrocenium redox couple ($E_{1/2}$ = 0.46 V) was used as an internal calibrant for the potential measurements.[65] Electron paramagnetic resonance (ESR) spectra were recorded on a Bruker EMX-8/2.7 (X-band) spectrometer at 77 K (liquid nitrogen). The ^{57}Fe Mössbauer spectra were recorded with a 2.5 × 10^{-2} C (9.25 × 10^8 Bq) ^{57}Co source using a symmetric triangular sweep mode. Computer fitting of the Mössbauer data to Lorentzian line shapes was carried out with a previously reported computer program.[71] The isomer shift values are reported relative to iron foil at 298 K. Elemental analyses were conducted on a Thermo-Finnigan Flash EA 1112 CHNS/O analyzer.

[1,4-{Cp*(dppe)Fe=C=CH}$_2$-2,5-(C≡CH)$_2$-C$_6$H$_2$](PF$_6$)$_2$ ([2-2H](PF$_6$)$_2$): A Schlenk tube was charged with 0.030 g (0.17 mmol) of freshly prepared 1,2,4,5-tetraethynylbenzene, 0.240 g (0.39 mmol, 2.3 equiv) of Cp*(dppe)FeCl (**3**), 0.060 g (0.39 mmol) of NH_4PF_6, and a 15 mL of MeOH/THF (2:1) mixture. The reaction mixture was stirred for 16 h at 20 °C. Then the solvents were evaporated and the solid residue was extracted with 20 mL of dichloromethane. The extracts were concentrated to 5 mL under reduced pressure. The product **[2-2H](PF$_6$)$_2$** was precipitated by addition of 15 mL of diethyl ether, filtered off, washed many times with 15 mL portions of diethyl ether to reach a colorless solution, and dried under vacuum to give 0.28 g (0.14 mmol, 87 % yield) of a yellow powder. Slow diffusion of pentane into a saturated CH_2Cl_2 solution of **[2-2H](PF$_6$)$_2$** afforded yellow crystals suitable for X-ray structure analysis. Anal. Calcd for $C_{86}H_{84}F_{12}P_6Fe_2$•2$CH_2Cl_2$: C, 58.30; H, 4.89. Found: C, 58.79; H, 4.72. FTIR (KBr, cm^{-1}): 2100 (w, $\nu_{C\equiv CH}$); 1617 (s, $\nu_{Fe=C=CH}$); 840 (s, ν_{PF}). ^{1}H NMR (400 MHz, CD_2Cl_2): 1.58 (s, 30 H, $C_5(CH_3)_5$); 2.50 (m, 4 H, CH_2); 3.08 (m, 4 H, CH_2); 3.12 (s, 2 H, C≡C-H); 5.62 (m, 2 H, Fe=C=CH); 6.14 (s, 2 H, H-3,6/C_6H_2); 7.17-7-63 (m, 40 H, Ph/dppe). ^{13}C{^{1}H} NMR (100 MHz, CD_2Cl_2): 10.2 ($C_5(\underline{C}H_3)_5$), 29.2 (t, $^1J_{C-P}$ = 22.0 Hz, PCH_2), 80.2 (C≡$\underline{C}$-H), 85.1 ($\underline{C}$≡C-H), 100.7 ($\underline{C}_5(CH_3)_5$), 116.1 (C-2,5-Ph), 122.4 (C=$\underline{C}$H), 129.2 and 129.4 (*m*-Ph/dppe), 131.7 (C-1,4-Ph), 132.4 (d, $^1J_{C-P}$ = 15.3 Hz, *ipso*-Ph/dppe), 131.2 and 131.3 (*p*-ph/dppe), 132.4 (d, $^1J_{C-P}$ = 11.1 Hz, *ipso*-Ph/dppe), 131.7 (*o*-Ph/dppe), 132.5 (C-3,6-Ph), 133.8 (t, *o*-Ph/dppe), 360.4 (t, $^2J_{C-P}$ = 33.0 Hz, Fe=$\underline{C}$). ^{31}P NMR (162 MHz, CD_2Cl_2): 86.20 (s, dppe); -144.38 (h, $^1J_{P-F}$ = 711.2 Hz, PF_6).

[1-{Cp*(dppe)Fe=C=CH}-2,5-(C≡CH)$_2$-4-{Cp*(dppe)Fe-C≡C}-C$_6$H$_2$](PF$_6$) ([2-H](PF$_6$)): Method A. A Schlenk tube was charged with a magnetic stir bar, 0.30 g (0.18 mmol) of the bisvinylidene derivative **[2-2H](PF$_6$)$_2$**, 0.022 g (0.20 mmol, 1.1 equiv) of potassium tert-butoxide and 30 mL of THF. The reaction mixture was stirred at 20 °C for 16 h. The solvent was removed under reduced pressure and the solid residue extracted with 2 x 20 mL of toluene. The solvent was evaporated and the solid material washed with 2 x 10 mL of pentane and dried under vacuum to give 0.27 g (0.18 mmol, 100% yield) of **[2-H](PF$_6$)** as a brown powder. Method B. A Schlenk tube was charged with a magnetic stir bar, 0.16 g (0.10 mmol) of the bisvinylidene derivative **[2-2H](PF$_6$)$_2$**, 0.13 g (0.10 mmol) of bis-iron(II) acetylide **2** and 20 mL of THF. The reaction mixture was stirred overnight at 20 °C. The solvent was removed under reduced pressure and the solid residue extracted with 2 x 20 mL of toluene. The solvent was evaporated and the solid material washed with 2 x 10 mL of pentane and dried under vacuum to give 0.29 g (0.20 mmol, 100% yield) of **[2-H](PF$_6$)** as a brown powder. FTIR (KBr, cm^{-1}): 2100 (w, $\nu_{C\equiv CH}$); 2028 (s, $\nu_{C\equiv C}$); 1568 (s, $\nu_{Fe=C=CH}$); 840 (s), ν(PF). ^{1}H NMR (400 MHz, C_6D_6): 1.49 (s, 15 H, Cp*Fe-C≡C); 1.44 (s, 15 H, Cp*Fe=C=CH-), 2.0 - 3.0 (mm, 10 H, CH_2 dppe, C≡CH), 6.96 (s, 2 H, H-3,6/C_6H_2); 7.0 - 8-03 (m, 40 H, Ph/dppe). ^{31}P NMR (162 MHz, C_6D_6): 99.8 (s, dppe Fe=C=CH-); 101.3 (s, dppe FeC≡C-); -144.38 (h, $^1J_{P-F}$ = 711.2 Hz, PF_6).

[1,4-{Cp*(dppe)FeC≡C}$_2$-2,5-(C≡CH)$_2$-C$_6$H$_2$] (2): A Schlenk tube was charged with a magnetic stir bar, 1.10 g (0.67 mmol) of the bisvinylidene derivative **[2-2H](PF$_6$)$_2$**, 0.18 g (1.67 mmol, 2.5 equiv) of potassium *tert*-butoxide and 100 mL of THF. Upon stirring at 20 °C for 16 h, the initial brown solution gradually turned orange. The solvent was then removed under reduced pressure and 10 mL of CH_2Cl_2 were added on the solid residue. The resulting suspension was washed with 2 x 1mL of water. Then the solvents were filtered off and the solid material washed with 10 mL of ethanol and 10 mL of pentane before being dried under vacuum to give **2** (0.60 g, 0.44 mmol, 66% yield) as an orange powder. HRMS (ESI$^+$): calcd for $C_{86}H_{82}P_4{}^{56}Fe_2$ (C$^+$): 1350.40604; found: 1350.4056. FT-IR (KBr, cm^{-1}): 2105 (vw, $\nu_{C\equiv CH}$); 2046 (s, $\nu_{C\equiv C}$). ^{1}H NMR (400 MHz, C_6D_6): 1.55 (s, Cp*). ^{31}P NMR (162 MHz, C_6D_6): 100.5 (s, dppe). The very low solubility of **2** did not permit a full analysis of the NMR spectra.

[1,4-{Cp*(dppe)FeC≡C}$_2$-2,5-(C≡CH)$_2$-C$_6$H$_2$](PF$_6$) (2(PF$_6$)): A Schlenk tube under argon, was charged with a magnetic stirbar, 0.25 g (0.18 mmol) of **2**, 0.06 g (0.18 mmol, 1 equiv) of ferrocenium

hexafluorophosphate and 10 mL of THF. The solution was stirred at 20 °C for 4 h, filtered and the solvent was removed under reduced pressure. The residue was washed with 2 × 30 mL portion of pentane and dried under vacuum overnight to give 0.17 g (0.11 mmol, 61% yield) of **2(PF$_6$)** as a green powder. HRMS (ESI$^+$): calcd for $C_{86}H_{82}F_6P_5{}^{56}Fe_2$ (C^{++}): 675.20275; found: 675.2030; (C^+): 1350.40604; found: 1350.4056. FT-IR (KBr, cm^{-1}): 2020 (m, $\nu_{FeC\equiv C}$); 1936 (s, $\nu_{FeC\equiv C}$); 1550 (m, ν_{aryl}); 840 (s, ν_{PF}).

[1,4-{Cp*(dppe)FeC≡C}$_2$-2,5-(C≡CH)$_2$-C$_6$H$_2$](PF$_6$)$_2$ (2(PF$_6$)$_2$): A Schlenk tube was charged with a magnetic stirbar, 0.31 g (0.19 mmol) of the bisvinylidene derivative **[2-2H](PF$_6$)$_2$**, 0.046 g (0.42 mmol, 2.5 equiv) of potassium *tert*-butoxide and 100 mL of THF. The reaction mixture was stirred at 20 °C for 16 h, upon which time the initial yellow solution gradually turned orange. Then 0.10 g (0.38 mmol; 2 equiv) of silver hexafluorophosphate was added and the solution was stirred at 20 °C for 4 additional hours. The solvent was removed under reduced pressure and the solid residue was then extracted with 2 x 50 ml of CH_2Cl_2. The solvent was evacuated under reduced pressure. The resulting green powder was washed with 2 × 30 mL portions of pentane and dried under vacuum overnight. The doubly oxidized complex **2(PF$_6$)$_2$** was obtained in 90 % yield (0.28 g, 0.17 mmol). Slow diffusion of pentane into a saturated CH_2Cl_2 solution of **2(PF$_6$)$_2$** afforded black-green crystals suitable for X-ray structure analysis. Anal. Calcd for $C_{86}H_{82}F_{12}P_6Fe_2{\bullet}CH_2Cl_2$: C, 58.36; H, 4.79. Found: C, 58.36; H, 4.75. HRMS (ESI$^+$): calcd for $C_{86}H_{82}P_4{}^{56}Fe_2$ (C^{++}): 675.20275; found: 675.2030; calcd for $C_{86}H_{82}F_6P_5{}^{56}Fe_2$ [C^{++}, PF_6^-]$^+$: 1495.37022; found: 1495.3695. FT-IR (KBr, cm^{-1}): 1947 (m, $\nu_{C\equiv C}$).

X-ray Crystal Structure Determinations: Well-shaped single crystals of **[2-2H](PF$_6$)$_2$•2CH$_2$Cl$_2$** and **2(PF$_6$)$_2$•2CH$_2$Cl$_2$** of suitable dimensions were coated in Paratone-N oil, mounted on a cryoloop and transferred to the cold gas stream of the cooling device. Intensity data for **[2-2H](PF$_6$)$_2$•2CH$_2$Cl$_2$** were collected on a APEXII, Bruker-AXS diffractometer, Mo-*K*α radiation (λ = 0.71073 Å), equipped with a bidimensional CCD detector, whereas those for **[2-H](PF$_6$)$_2$•2CH$_2$Cl$_2$** were collected on a D8 VENTURE Bruker-AXS diffractometer equipped with a multilayer monochromated Mo-*K*α radiation (λ = 0.71073 Å) and a CMOS Photon100 detector. In both cases, intensity data were collected at *T* = 150(2) K and corrected for absorption effects using multiscanned reflections. The two structures were solved by a dual-space algorithm using the SHELXT program,[105] and then refined with full-matrix least-square method based on F^2 (SHELXL-2014).[106] All non-hydrogen atoms were refined with anisotropic atomic displacement parameters. All the hydrogen atoms were placed in their geometrically idealized positions and constrained to ride on their parent atoms. A summary of the details about crystal data, collection parameters and refinement are documented in Table S1 (Supporting Information), and additional crystallographic details are provided in the CIF file. ORTEP views were drawn using OLEX2 software.[107] CCDC 1977935 for **[2-2H](PF$_6$)$_2$•2CH$_2$Cl$_2$** and 1977889 for **2(PF$_6$)$_2$•2CH$_2$Cl$_2$** contain the full crystallographic data for this paper. These data can be obtained free of charge from The Cambridge Crystallographic Data Centre via www.ccdc.cam.ac.uk/data_request/cif.

Computational Details: Density-functional theory (DFT) calculations were performed using the Gaussian 09 program package.[108] Full geometry optimizations were carried out without any symmetry constraint using the PBE0 functional[109] within the Def2-SVP basis set for iron atoms and 6-31+G* for the other ones. Computations of the magnetic states of the dicationic species were realized with the Amsterdam Density Functional (ADF) program using the ADF triple-ζ quality basis set[110-112] on geometries optimized via Gaussian 09. Electron correlation was treated within the local density approximation (LDA) in the Vosko−Wilk−Nusair parametrization.[113] Nonlocal corrections were added to the exchange and correlation energies using the PBE0 functional.[109] Molecular structures, orbitals and Mulliken spin densities were plotted using the GaussView program.[114] Orbital compositions were obtained using the AOMix program.[115, 116]

Acknowledgments

T. G., S. K. and J.-F. H. thank GENCI (Grand Equipment National de Calcul Intensif) for HPC resources project GENCI A0030807367).

Keywords: ironacetylide • mixed-valence • electronic coupling • magnetic coupling • bridge-centered radical

[1] N. Robertson, G. A. Mc Gowan, *Chem. Soc. Rev.* **2003**, *32*, 96.

[2] A. C. Benniston, *Chem. Soc. Rev.* **2004**, *33*, 573.

[3] A. H. Flood, J. F. Stoddart, D. W. Steuerman, J. R. Heath, *Science* **2004**, *306*, 2055.

[4] M. C. Petty, *Molecular Electronics: From Principles to Practice*, Wiley, New York, **2008**.

[5] D. M. D'Alessandro, F. R. Keene, *Chem. Soc. Rev.* **2006**, *35*, 424.

[6] S. Záliš, R. F. Winter, W. Kaim, *Coord. Chem. Rev.* **2010**, *254*, 1383.

[7] F. Paul, C. Lapinte, *Coord. Chem. Rev.* **1998**, *178-180*, 427.

[8] J.-F. Halet, C. Lapinte, *Coord. Chem. Rev.* **2013**, *257*, 1584.

[9] P. J. Low, *Dalton Trans.* **2005**, 2821.

[10] N. Le Narvor, C. Lapinte, *J. Chem. Soc., Chem. Commun.* **1993**, 357.

[11] N. Le Narvor, L. Toupet, C. Lapinte, *J. Am. Chem. Soc.* **1995**, *117*, 7129.

[12] M. Guillemot, L. Toupet, C. Lapinte, *Organometallics* **1998**, *17*, 1928.

[13] M. Brady, W. Weng, Y. Zhou, J. W. Seyler, A. J. Amoroso, A. M. Arif, M. Böhme, G. Frenking, J. A. Gladysz, *J. Am. Chem. Soc.* **1997**, *119*, 775.

[14] H. Jiao, K. Costuas, J. A. Gladysz, J.-F. Halet, M. Guillemot, L. Toupet, F. Paul, C. Lapinte, *J. Am. Chem. Soc.* **2003**, *125*, 9511.

[15] M. I. Bruce, L. I. Denisovich, P. J. Low, S. M. Peregudova, N. A. Ustynyuk, *Mendeleev Commun.* **1996**, 200.

[16] M. I. Bruce, P. J. Low, K. Costuas, J.-F. Halet, S. P. Best, G. A. Heath, *J. Am. Chem. Soc.* **2000**, *122*, 1949.

[17] M. I. Bruce, B. G. Ellis, P. J. Low, B. W. Skelton, A. H. White, *Organometallics* **2003**, *22*, 3184.

[18] M. I. Bruce, K. Costuas, T. Davin, B. E. Ellis, J.-F. Halet, C. Lapinte, P. J. Low, K. M. Smith, B. W. Skelton, L. Toupet, A. H. White, *Organometallics* **2005**, *24*, 3864.

[19] K. Venkatesan, O. Blacque, H. Berke, *Dalton Trans.* **2007**, 1091.

[20] S. N. Semenov, O. Blacque, T. Fox, K. Venkatesan, H. Berke, *J. Am. Chem. Soc.* **2010**, *132*, 3115.

[21] J. B. G. Gluyas, S. Gückel, M. Kaupp, P. J. Low, *Chem. Eur. J.* **2016**, *22*, 16138.

[22] F. Gendron, T. Groizard, B. Le Guennic, J.-F. Halet, *Eur. J. Inorg. Chem.* **2020**, 667.

[23] J. P. Launay, *Eur. J. Inorg. Chem.* **2020**, 329.
[24] P. F. H. Schwab, M. D. Levin, J. Michl, *Chem. Rev.* **1999**, *99*, 1863.
[25] P. F. H. Schwab, M. D. Levin, J. Michl, *Chem. Rev.* **2005**, *105*, 1197.
[26] M. I. Bruce, P. J. Low, *Adv. Organomet. Chem.* **2004**, *50*, 179.
[27] S. Szafert, J. A. Gladysz, *chem. Rev.* **2003**, *103*, 4175.
[28] S. Szafert, J. A. Gladysz, *Chem. Rev.* **2006**, *106*, PR1.
[29] J. P. Launay, *Coord. Chem. Rev.* **2013**, *257*, 1544.
[30] P. J. Low, *Coord. Chem. Rev.* **2013**, *257*, 1507.
[31] Y. Lu, R. Quardokus, C. S. Lent, F. Justaud, C. Lapinte, S. A. Kandel, *J. Am. Chem. Soc.* **2010**, *132*, 13519.
[32] R. C. Quardokus, Y. Lu, N. A. Wasio, C. S. Lent, F. Justaud, C. Lapinte, S. A. Kandel, *J. Am. Chem. Soc.* **2012**, *134*, 1710.
[33] K. Costuas, S. Rigaut, *Dalton Trans.* **2011**, *40*, 5643.
[34] S. Marques-Gonzalez, D. S. Yufit, J. A. K. Howard, S. Martin, H. M. Osorio, V. M. Garcia-Suarez, R. J. Nichols, S. J. Higgins, P. Cea, P. J. Low, *Dalton Trans.* **2013**, *42*, 338.
[35] F. Schwarz, G. Kastlunger, F. Lissel, H. Riel, K. Venkatesan, H. Berke, R. Stadler, E. Lörtscher, *Nano Lett.* **2014**, *14*, 5932.
[36] O. A. Al-Owaedi, D. C. Milan, M.-C. Oerthel, S. Bock, D. S. Yufit, J. A. K. Howard, S. J. Higgins, R. J. Nichols, C. J. Lambert, M. R. Bryce, P. J. Low, *Organometallics* **2016**, *35*, 2944.
[37] S. Bock, O. A. Al-Owaedi, S. G. Eaves, D. C. Milan, M. Lemmer, B. W. Skelton, H. M. Osorio, R. J. Nichols, S. J. Higgins, P. Cea, N. J. Long, T. Albrecht, S. Martin, C. J. Lambert, P. J. Low, *Chem. Eur. J.* **2017**, *23*, 2133.
[38] D. C. Milan, A. Vezzoli, I. J. Planje, P. J. Low, *Dalton Trans.* **2018**, *47*, 14125.
[39] S. N. Natoli, T. J. Azbell, P. E. Fanwick, M. Zeller, T. Ren, *Organometallics* **2016**, *35*, 3594.
[40] W. P. Forrest, M. M. R. Choudhuri., S. M. Kilyanek, S. N. Natoli, B. M. Prentice, P. E. Fanwick, R. J. Crutchley, T. Ren, *inorg. Chem.* **2015**, *54*, 7645.
[41] J. B. G. Gluyas, V. Manici, S. Gückel, K. B. Vincent, D. S. Yufit, J. A. K. Howard, B. W. Skelton, A. Beeby, M. Kaupp, P. J. Low, *J. Org. Chem.* **2015**, *80*, 11501.
[42] R. Makhoul, J. B. G. Gluyas, K. B. Vincent, H. Sahnoune, J.-F. Halet, P. J. Low, J.-R. Hamon, C. Lapinte, *Organometallics* **2018**, *37*, 4156.
[43] M. Lohan, F. Justaud, T. Roisnel, P. Ecorchard, H. Lang, C. Lapinte, *Organometallics* **2010**, *29*, 4804.
[44] M. Lohan, F. Justaud, H. Lang, C. Lapinte, *Organometallics* **2012**, *31*, 3565.
[45] Y. Tanaka, J. A. Shaw-Taberlet, F. Justaud, O. Cador, T. Roisnel, M. Akita, J.-R. Hamon, C. Lapinte, *Organometallics* **2009**, *28*, 4656.
[46] Y. Tanaka, T. Ishisaka, A. Inagaki, T. Koike, C. Lapinte, M. Akita, *Chem. Eur. J.* **2010**, *16*, 4762.
[47] A. J. Zucchero, P. L. Mcgrier, U. H. F. Bunz, *Acc. Chem. Res.* **2010**, *43*, 397.
[48] M. Gholami, R. R. Tykwinski, *Chem. Rev.* **2006**, *106*, 4997.
[49] M. I. Bruce, A. Burgun, M. A. Fox, M. Jevric, P. J. Low, B. K. Nicholson, C. R. Parker, B. W. Skelton, A. H. White, N. N. Zaitseva, *Organometallics* **2013**, *32*, 3286.
[50] M. Akita, T. Koike, *Dalton Trans.* **2008**, 3523.
[51] M. Linseis, R. F. Winter, B. Sarkar, W. Kaim, S. Za'lis, *Organometallics* **2008**, *27*, 3321.
[52] M. Akita, Y. Tanaka, C. Naitoh, T. Ozawa, N. Hayashi, M. Takeshita, A. Inagaki, M.-C. Chung, *Organometallics* **2006**, *25*, 5261.
[53] G. T. Dalton, M. P. Cifuentes, S. Petrie, R. Stranger, M. G. Humphrey, M. Samoc, *J. Am. Chem. Soc.* **2007**, *129*, 11882.
[54] V. N. Nemykin, G. T. Rohde, C. D. Barrett, R. G. Hadt, C. Bizzarri, P. Galloni, B. Floris, I. Nowik, R. H. Herber, A. G. Marrani, R. Zanoni, N. M. Loim, *J. Am. Chem. Soc.* **2009**, *131*, 14969.
[55] G. Grelaud, M. P. Cifuentes, F. Paul, M. G. Humphrey, *J. Organomet. Chem.* **2014**, *751*, 181.
[56] C. S. Lent, *Science* **2000**, *288*, 1597.
[57] T. Groizard, S. Kahlal, J.-F. Halet, *J. Organomet. Chem.* **2017**, *844*, 35.
[58] R. Makhoul, P. Hamon, T. Roisnel, J.-R. Hamon, C. Lapinte, *Chem. Eur. J.* **2020**, doi.org/10.1002/chem.202000910.
[59] A. A. Kocherzhenko, L. D. A. Siebbeles, F. C. Grozema, *J. Phys. Chem. Lett.* **2011**, *2*, 1753.
[60] N. Le Narvor, C. Lapinte, *Organometallics* **1995**, *14*, 634.
[61] R. Makhoul, H. Sahnoune, V. Dorcet, J.-F. Halet, J.-R. Hamon, C. Lapinte, *Organometallics* **2015**, *34*, 3314.
[62] N. G. Connelly, M. P. Gamasa, J. Gimeno, C. Lapinte, E. Lastra, J. P. Maher, N. Le Narvor, A. L. Rieger, P. H. Rieger, *J. Chem. Soc., Dalton Trans.* **1993**, 2575.
[63] M. I. Bruce, *Chem. Rev.* **1991**, *91*, 197.
[64] A. J. Bard, L. R. Faulkner, *Electrochemical Methods: fundamentals and applications*, 2nd ed., John Wiley & Sons Inc., New York, **2000**.
[65] N. G. Connelly, W. E. Geiger, *Chem. Rev.* **1996**, *96*, 877.
[66] G. Argouarch, P. Thominot, F. Paul, L. Toupet, C. Lapinte, *C. R. Chimie* **2003**, *6*, 209.
[67] P. Gamasa, J. Gimeno, E. Lastra, B. M. Martin, A. Anillo, A. Tiripicchio, *Organometallics* **1992**, *11*, 1373.
[68] K. Costuas, F. Paul, L. Toupet, J.-F. Halet, C. Lapinte, *Organometallics* **2004**, *23*, 2053.
[69] F. Paul, L. Toupet, J.-Y. Thépot, K. Costuas, J.-F. Halet, C. Lapinte, *Organometallics* **2005**, *24*, 5464.
[70] E. C. Fitzgerald, A. Ladjarafi, N. J. Brown, D. Collison, K. Costuas, R. Edge, J.-F. Halet, F. Justaud, P. J. Low, H. Meghezzi, T. Roisnel, M. W. Whiteley, C. Lapinte, *Organometallics* **2011**, *30*, 4180.
[71] F. Varret, J.-P. Mariot, J.-R. Hamon, D. Astruc, *Hyperfine Interact.* **1988**, *39*, 67.
[72] V. Guillaume, P. Thominot, F. Coat, A. Mari, C. Lapinte, *J. Organomet. Chem.* **1998**, *565*, 75.
[73] S. Roué, H. Sahnoune, L. Toupet, J.-F. Halet, C. Lapinte, *Organometallics* **2016**, *35*, 2057.
[74] V. Guillaume, V. Mahias, A. Mari, C. Lapinte, *Organometallics* **2000**, *19*, 1422.
[75] S. Le Stang, F. Paul, C. Lapinte, *Organometallics* **2000**, *19*, 1035.
[76] R. J. Webb, T.-Y. Dong, C. P. Pierpont, S. R. Boone, R. K. Chadha, D. N. Hendrickson, *J. Am. Chem. Soc.* **1991**, *113*, 4806.
[77] T.-Y. Dong, T. Kambara, D. N. Hendrickson, *J. Am. Chem. Soc.* **1986**, *108*, 4423.

[78] T.-Y. Dong, T. Kampara, D. N. Hendrickson, *J. Am. Chem. Soc.* **1986**, *108*, 5857.

[79] M. D. Lowery, W. S. Hammack, H. G. Drickamer, D. N. Hendrickson, *J. Am. Chem. Soc.* **1987**, *109*, 8919.

[80] M. A. Fox, B. Le Guennic, R. L. Roberts, D. A. Brue, D. S. Yufit, J. A. K. Howard, G. Manca, J.-F. Halet, F. Hartl, P. J. Low, *J. Am. Chem. Soc.* **2011**, *133*, 18433.

[81] K. Costuas, O. Cador, F. Justaud, S. Le Stang, F. Paul, A. Monari, S. Evangelisti, L. Toupet, C. Lapinte, J.-F. Halet, *Inorg. Chem.* **2011**, *50*, 12601.

[82] T.-Y. Dong, C.-C. Sohel, M.-Y. Hwang, T. Y. Lee, S.-K. Yeh, Y.-S. Wen, *Organometallics* **1992**, *11*, 573.

[83] S. I. Ghazala, F. Paul, L. Toupet, T. Roisnel, P. Hapiot, C. Lapinte, *J. Am. Chem. Soc.* **2006**, *128*, 2463.

[84] R. Denis, L. Toupet, F. Paul, C. Lapinte, *Organometallics* **2000**, *19*, 4240.

[85] S. Le Stang, F. Paul, C. Lapinte, *Inorg. Chim. Acta* **1999**, *291*, 403.

[86] M. B. Robin, P. Day, *Adv. Inorg. Chem. Radiochem.* **1968**, *10*, 247.

[87] S. Ernst, P. Hänel, J. Jordanov, W. Kaim, V. Kasack, *J. Am. Chem. Soc.* **1989**, *111*, 1733.

[88] S. B. Piepho, E. R. Krausz, P. N. Schatz, *J. Am. Chem. Soc.* **1978**, *100*, 2996.

[89] J.-P. Launay, C. Coudret, C. Hortholary, *J. Phys. Chem. B* **2007**, *111*, 6788.

[90] H. Sahnoune, V. Mahias, J.-F. Halet, C. Lapinte, *Organometallics* **2019**, *28*, 2724.

[91] K. D. Demandis, C. M. Hartshorn, T. J. Meyer, *Chem. Rev.* **2001**, *101*, 2655.

[92] N. S. Hush, *Trans. Faraday Soc.* **1961**, *57*, 557.

[93] N. S. Hush, *Prog. Inorg. Chem.* **1967**, *8*, 391.

[94] C. Roger, P. Hamon, L. Toupet, H. Rabaâ, J.-Y. Saillard, J.-R. Hamon, C. Lapinte, *Organometallics* **1991**, *10*, 1045.

[95] F. Paul, A. Bondon, G. Da Costa, F. Malvoti, S. Sinbandit, O. Cador, K. Costuas, L. Toupet, M. L. Boillot, *Inorg. Chem.* **2009**, *48*, 10608.

[96] N. Le Narvor, C. Lapinte, *C. R. Acad. Sci., Paris, t. 1, série IIc* **1998**, 745.

[97] T. Weyland, K. Costuas, A. Mari, J.-F. Halet, C. Lapinte, *Organometallics* **1998**, *17*, 5569.

[98] S. Roué, S. Le Stang, L. Toupet, C. Lapinte, *C. R. Chimie* **2003**, *6*, 353.

[99] A. Burgun, F. Gendron, C. Sumby, T. Roisnel, O. Cador, K. Costuas, J.-F. Halet, M. I. Bruce, C. Lapinte, *Organometallics* **2014**, *33*, 2613.

[100] C. Lapinte, *J. Organomet. Chem.* **2008**, *693*, 793.

[101] M. Wicholas, R. Mustacich, D. Jayne, *J. Am. Chem. Soc.* **1972**, *94*, 4518.

[102] O. Kahn, *Molecular Magnetism*, VCH Publishers, New York, **1993**.

[103] I. Bertini, C. Luchinat, *NMR of Paramagnetic Molecules in Biological Systems*, The Benjamin/Cummings Publishing Company, Inc. ed., Menlo Park, California, **1986**.

[104] B. C. Berris, G. H. Hovakeemian, Y.-H. Lai, K. P. C. Vollhardt, *J. Am. Chem. Soc.* **1986**, *107*, 5670.

[105] G. M. Sheldrick, *Acta Crystallogr. Sect. A* **2015**, *71*, 3.

[106] G. M. Sheldrick, *Acta Crystallogr. Sect. C* **2015**, *71*, 3.

[107] O. V. Dolomanov, L. J. Bourhis, R. J. Gildea, J. A. K. Howard, H. Puschmann, *J. Appl. Crystallogr.* **2009**, *42*, 339.

[108] M. J. Frisch, G. W. Trucks, H. B. Schlegel, G. E. Scuseria, M. A. Robb, J. R. Cheeseman, G. Scalmani, V. Barone, B. Mennucci, G. A. Petersson, H. Nakatsuji, M. Caricato, X. Li, H. P. Hratchian, A. F. Izmaylov, J. Bloino, G. Zheng, J. L. Sonnenberg, M. Hada, M. Ehara, K. Toyota, R. Fukuda, J. Hasegawa, M. Ishida, T. Nakajima, Y. Honda, O. Kitao, H. Nakai, T. Vreven, J. Montgomery, J. A., J. E. Peralta, F. Ogliaro, M. Bearpark, J. J. Heyd, E. Brothers, K. N. Kudin, V. N. Staroverov, R. Kobayashi, J. Normand, K. Raghavachari, A. Rendell, J. C. Burant, S. S. Iyengar, J. Tomasi, M. Cossi, N. Rega, N. J. Millam, M. Klene, J. E. Knox, J. B. Cross, V. Bakken, C. Adamo, J. Jaramillo, R. Gomperts, R. E. Stratmann, O. Yazyev, A. J. Austin, R. Cammi, C. Pomelli, J. W. Ochterski, R. L. Martin, K. Morokuma, V. G. Zakrzewski, G. A. Voth, P. Salvador, J. J. Dannenberg, S. Dapprich, A. D. Daniels, Ö. Farkas, J. B. Foresman, J. V. Ortiz, J. Cioslowski, D. J. Fox, *Gaussian 09*, *Revision A.02;* Gaussian Inc., Wallingford, CT, **2009**.

[109] V. Vetere, C. Adamo, P. Maldivi, *Chem. Phys. Lett.* **2000**, *325*, 99.

[110] G. te Velde, F. M. Bickelhaupt, S. J. A. van Gisbergen, C. Fonseca Guerra, E. J. Baerends, J. G. Snijders, T. Ziegler, *J. Comput. Chem.* **2001**, *22*, 931.

[111] C. Fonseca Guerra, J. G. Snijders, G. te Velde, E. J. Baerends, *J. Theor. Chem. Acc.* **1998**, *99*, 391.

[112] ADF2014.07, SCM, Theoretical Chemistry, Vrije Universiteit, Amsterdam, The Netherlands, http://www.scm.com.

[113] S. H. Vosko, L. Wilk, M. Nusair, *Can. J. Phys.* **1980**, 1200.

[114] R. Dennington, K. T. Millam, *Version 5* ed. (Ed.: *GaussView*), J. Semichem Inc.,, Shawnee Mission, KS, **2009**.

[115] S. I. Gorelsky, in *SWizard Program; http://www.sg-chem.net*, University of Ottawa, **2007**.

[116] S. I. Gorelsky, A. B. P. Lever, *J. Organomet. Chem.* **2001**, *635*, 187.

10.1002/ejic.202000345

WILEY-VCH

FULL PAPER

The new complex [1,4-{Cp*(dppe)Fe-C≡C}$_2$-2,5-(C≡CH)$_2$-C$_6$H$_2$] (**2**) was selectively obtained from the reaction of 1,2,4,5--tetraethynylbenzene with two equiv of Cp*(dppe)FeCl and subsequent deprotonation. The ethynyl groups located at the 2,5 positions of the aromatic ring of the bridge play a sizeable role on the electronic and magnetic couplings of the oxidized forms **2(PF$_6$)** and **2(PF$_6$)$_2$**.

Molecular Electronics

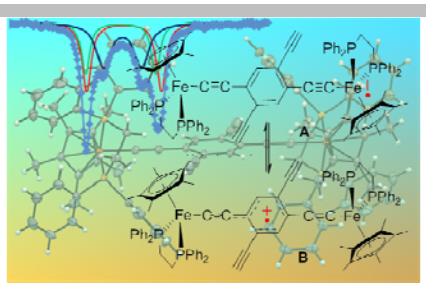

Rim Makhoul, Thomas Groizard, Paul Hamon, Thierry Roisnel, Vincent Dorcet, Samia Kahlal, Jean-François Halet, Jean-René Hamon,* and Claude Lapinte**

Page No. – Page No.

1,4-Diethynylbenzene-Bridged [Cp*(dppe)Fe]n+ Units: Effect of 2,5-Ethynyl Groups on the Chemical and Electronic Properties